How sustainable is CO_2 conversion to ethanol? – a life cycle assessment of a new electrocatalytic carbon utilisation process

Supplementary information

Daniel Rojas Sánchez[†]; Kaveh R. Khalilpour[‡], Andrew F.A. Hoadley[†]

[†]*Department of Chemical Engineering, Monash University, Melbourne, VIC 3800, Australia*

[‡]*Faculty of Engineering and IT, University of Technology Sydney, Sydney, NSW 2007, Australia*

Table of Contents

Tables

Figures

S1. Life cycle inventory

S1.1 General inventory considerations

All background processes for the life cycle inventory (LCI) data come from two databases: the Australian Life Cycle Initative (AusLCI) database V1.35 (Australian Life Cycle Assessment Society, 2020) and ecoinvent 3.5 (Wernet et al., 2016).

Unless otherwise noted, different processes assume Australian conditions. Key transportation distances were modified to better represent the area of study. However, general or universal processes may be based on transportation distances for materials in Europe, as reported in the ecoinvent database. Whenever distances are unknown, transport is assumed to be a standard distance of 100km for Lorry >16t and 600km for freight rail, as used throughout the AusLCI database. Whenever a transport requirement is not directly input, it means it is included within the process of the material requirement itself.

Waste and emissions of the end of life of each manufacture process are included in full within its inventory. When a process needs an equipment or chemical manufactured, its required mass, unit, area, or volume will be normalised according to its lifetime. Operation hours for plants are assumed 8,000 hours in a year, as per industry standard.

S1.2 Electrolyser stack

The electrolyser was modelled according to the description in Section S2.1. It was first scaled-up to 2 m^2, which is the area of the electrode in an advanced large-scale alkaline electrolyser, as described in Koj et al. (2015). The process for scaling the inventory requirements is described in Section S1.2.1 and in subsequent inventories for subcomponents. Then, the electrolyser was scaled-out by creating stacks to match the output of the reference system. Up to 15,429 assembled electrolysers are needed to produce the necessary ethanol flow.

The electrolyser stack was assumed to be rows of assembled electrolysers stacks. The design of the electrolyser assembly allows stacking them as a wall: on one side inputs of electrolyte and gas and, on the other, its corresponding outputs. To reinforce the modular advantage of these electrolyser cells, stacks were designed to fit into a standard 40ft container (12.2 m x 2.4 m x 2.6 m). With these dimensions, 31 containers are needed, each with seven electrolysers in a row and 72 stacked in each column. The area needed within the plant is calculated from the number of containers needed, assuming they are positioned abreast and three can be stacked on top of each other. An added 15% of this area is added to cover the space needed for pumps, valves, and pipelines. This total area required is linked to transformation, while the occupation is based on the lifetime of the entire stack.

Alkaline electrolysis cell stacks can have a lifetime of 60,000 – 90,000 hours (Schmidt et al., 2017). To take a conservative approach and given that voltage degradation starts to happen at the lower end of that range in low-temperature alkaline systems (Bertuccioli et al., 2014), the lifetime of the electrolyser stack was assumed 60,000 hours. Therefore, the lifetimes of the membrane, gas diffusion layer, anode, and electrolyte will be 60,000 hours of operation, consistent with the LCA by Rumayor et al. (2019) The lifetime of the frame and other components outside of the stack are assumed 20 years, which is the lower end of the lifetime of alkaline electrolysis systems described in Carmo et al. (2013).

The stability of the cathode has been tested, but there is not sufficient experimental data for this specific electrode to estimate its lifetime at a larger scale. In this model we assume the lifetime to be 5000 hours, being the average stack lifetime of polymer electrolyte membrane fuel cells, which have considerably shorter lifespan than alkaline systems (Myers et al., 2012). The inventory for the electrolyser stack is shown in Table S1.

Table S1. Inventory for the electrolyser stack

Parameter	Amount
Functional unit output	
Electrolyser stack [unit]	1
Material requirements	
Assembled electrolyser [unit]	15429
Infrastructure requirements	
Occupation, industrial area [m^2a]	2609.6
Transformation, from unknown [m^2]	347.9
Transformation, to industrial area [m^2]	347.9

S1.2.1 Manufacture of assembled electrolyser

The build of the flow cell electrolyser is shown in Wang et al. (2020) and schematised in Li et al. (2020) The prepared cathode electrode, gas diffusion layer (GDL), anion exchange membrane (AEM), and Ni foam anode are clamped and assembled using polytetrafluoroethylene (PTFE) spacers. The inventories for the mentioned elements are given in later subsections. The frame of the cell consists of compression plates and bolts holding together the cell assembly. The frame is assumed to be low-alloy steel plates compressed with 8, ¼ inch bolts, as manufactured in Li and Oloman (2005) for a conservative approach. However, using 3D printed cheaper thermoplastics, as polylactic acid in Hudkins et al. (2016) would result in cheaper manufacturing with potentially lower environmental impacts. The lifetime of the frame is assumed 20 years, being possible to replace the electrolyser stack at the end of its lifetime (60,000 hours) and keep using the same frame.

The material requirements follow the necessary components normalised to the lifetime of the frame. The PTFE spacers are estimated to double the dimension of the longer side of the membrane according to the schematic of the flow cell in the mentioned references. The PTFE spacer thickness is assumed to be 1.5 mm as the average thickness of spacers commercialised by Klinger Australia (n.d.). The area of the plates are the sum of the membrane and the gasket. The depth of the cell (3.0 cm) and thickness of the steel plates (0.3 cm) are taken from Hudkins et al. (2016). Bolts are assumed ¼'' x 1 ¼'' steel, with one in each corner of the frame.

The energy requirements for the frame are embodied by the steel manufacturing process. For the assembly, the electricity per square meter defined by Duclos et al. (2017) is used. Transport requirements are neglected since assembly is assumed to happen on-site. Infrastructure requirements are not allocated to this inventory since they are aggregated with the adsorption and distillation system. Waste and emissions are associated with the end of life disposal of each component considered in their corresponding inventory, with the exception of the disposal of the frame that is specified here.

As previously mentioned, the electrolyser was scaled by increasing the size of the electrode area to 2 m^2. The side of the spacers in the scaled-up electrolyser was assumed to be 1.2 times the length of the electrode rather than double as in the original lab-scale design. This was assumed as an improved design efficiency, using a relatively lower amount of PTFE for the gasket and steel for the frame. The thickness of the frame and electrolyser was kept identical. The detailed inventory is shown in Table S2.

Table S2. Inventory for the assembled electrolyser

Parameter	Amount
Functional unit output	
Assembled electrolyser [unit]	1
Material requirements	
PTFE [kg]	0.54
Low-alloyed steel, frame [kg]	117.54
Low-alloyed steel, bolts [kg]	0.78
N-C/Cu electrode [m^2]	64.00
Ni foam [kg]	1.85
Anion exchange membrane [m^2]	5.33
Gas diffusion layer [m^2]	5.33
KOH electrolyte 1M [kg]	1680.00
Steel product manufacturing [kg]	117.54
Energy and processing requirements	
Assembly, electricity [MJ]	32.03
Waste and emissions	
Disposal of steel to landfill [kg]	118.32
Plastics, mixture, to sanitary landfill	0.54

S1.2.2 Manufacture of N-C/Cu electrode

The N-C/Cu electrode was synthesised by sputtering a 200nm layer of copper nanoparticles as catalyst onto a PTFE membrane, followed by a 50nm layer of nitrogen-doped carbon (N-C) using a magnetron sputtering system. The specific nitrogen content of the N-C layer is 34%.

The material requirements were calculated from the experimental procedure assuming stoichiometric quantities. The PTFE membrane used in the catalyst synthesis was purchased from Beijing Zhongxingweiye Instrument Co., Ltd. This product has a specified thickness range of 198.1 – 269.2 μm. In this inventory, the average thickness was used to calculate the mass of PTFE needed. The mass of PTFE required was calculated by taking as base the density of the PTFE membrane commercialised by Microlab Scientific (n.d.) with a weight of 30 g/m^2 and a thickness of 122 μm.

Since no specifications are given, the associated energy requirements of a sputtering process of indium tin oxide for liquid crystal display in ecoinvent (modified with AusLCI data) and the transport of its targets were used as a proxy, adapting the quantity to the specific dimensions of each layer. The process for copper layering in ecoinvent specifies a 50% efficiency of the targets, so material requirements were increased to consider this loss. The infrastructure requirements are standard from ecoinvent guidelines. Due to lack of data, no direct material losses or emissions are associated to this process other than the disposal and recycling of material lost and waste heat. The disposal of a catalyst for ethylene dichloride production is used as a proxy for the end of life of this catalyst as hazardous waste incineration. A detailed inventory can be found in Table S3.

Table S3. Inventory for the manufacture of N-C/Cu electrode

Parameter	Amount
Functional unit output	
N-C/Cu electrode [m^2]	1
Material requirements	
PTFE [kg]	0.057
Copper, primary [kg]	0.004
Nitrogen, at plant [kg]	0.0005
Argon, at plant [kg]	0.0022
Graphite, battery grade, at plant [kg]	0.0008
Energy and processing requirements	
Electricity for sputtering [kWh]	7.319
Transport requirements	
Freight aircraft transport [tkm]	0.0090
Lorry >16t [tkm]	0.0002
Infrastructure requirements	
Facilities for production [kg]	1.47E-04
Chemical plant [unit]	4.00E-10
Waste and emissions	
Disposal of copper [kg]	0.0019
Carbon, as graphite [kg]	0.0004
Nitrogen [kg]	0.0002
Argon [kg]	0.0011
Disposal of catalyst (proxy with catalyst for EDC production) [kg]	0.0600
Waste heat [MJ]	26.35

S1.2.3 Manufacture of Ni foam catalyst

Nickel foam is a porous material with high electronic conductivity and surface area, typically manufactured by electrodeposition or chemical vapour deposition of nickel ions as coating on a polymer (Chaudhari et al., 2017). The specific Ni foam used as anode catalyst in Wang et al. (2020) is commercially produced by MTI Corporation (product number: Eq-bcnf-16m). Given the manufacturing details of this Ni foam are not publicly available, the electrodeposition of nickel ions in the form of $NiSO_4$ on polyurethane foam from Liu and Liang (2000) is assumed.

The material requirements were calculated from the information available for this product (namely, surface density of 346 g/cm^2 and a thickness of 1.6 mm^2). The energy, transport, and infrastructure requirements and emissions are based on the LCA of Ni metal hydride electrode substrate in batteries of electric vehicles by Majeau-Bettez et al. (2011). The disposal of nickel at its end of life is approximated using the AusLCI process Disposal of copper with 0% water to municipal incineration. The detailed inventory is shown in Table S4.

Table S4. Inventory for the manufacture of Ni foam

Parameter	Amount
Functional unit output	
Ni foam, at plant [kg]	1
Material requirements	
Nickel, 99.5%, GLO (proxy for electroplated NiSO4) [kg]	1
Polyurethane, flexible foam [kg]	0.028
Energy and processing requirements	
Heat, unspecific, in chemical plant (burn-off polyurethane) [MJ]	0.078
Heat, unspecific, in chemical plant (sinter) [MJ]	1.5
Transport requirements	
Freight rail transport [tkm]	0.61
Lorry >16t [tkm]	0.10
Infrastructure requirements	
Chemical plant [unit]	4.0E-10
Waste and emissions	
Waste polyurethane, open burning (proxy for combustion) [kg]	0.028
Waste heat [MJ]	1.578
Disposal of nickel to incineration [kg]	1

S1.2.4 Manufacture of anion exchange membrane

Anion exchange membranes (AEM) are generally composed of a polymer as main structure with cationic sites that allow the pass of hydroxide ions and other anions between anode and cathode (Pan et al., 2018). The specific AEM used in the flow cell electrolyser of Wang *et al.*(Wang et al., 2020) is the commercial product Fumasep FAB-PK-130 (product code: 5041636) manufactured by Fuel Cell Store. Although the Technical Sheet for this product has a comprehensive characterisation of its conductivity and strength properties, there is not sufficient information on its composition or manufacture process. Therefore, we used the synthesis of an imidazolium functionalised polysulfone AEM as designed by Zhang et al. (2011) as proxy, since their membrane has comparable conductive properties.

The material requirements were calculated based on the experiment of Zhang et al. (2011). The energy requirements were calculated by the thermodynamic heating and boil-off of the solvents and unreacted chemicals in the experiment, neglecting the power needed for the stirring involved. As in Simons and Bauer (2015), the energy requirements and waste/emissions of extrusion to plastic films were added as a proxy for its industrial manufacture, relating the needed fraction according to the weight of the membrane as plastic. The weight of the membrane was determined to be 3.34 $mg \cdot cm^{-2}$ according to the calculated molecular weight of the membrane, the stoichiometry of the reactions, and the area of the membrane produced. Transport and infrastructure requirements are standard from ecoinvent guidelines. No pre-treatment losses were considered. The waste and emissions are carried from the extrusion process, except the disposal of the membrane that is taken from the ecoinvent process *Spent anion exchange resin from potable water production* as a proxy. The detailed inventory is presented in Table S5.

Table S5. Inventory for the manufacture of the anion exchange membrane

Parameter	Amount
Functional unit output	
Anion exchange membrane, at plant [m^2]	1
Material requirements	
Polysulfone [kg]	0.021
Chloromethylmethylether (CMME) [kg]	0.035
N-N Dimethylacetamide (DMAc) [kg]	0.468
Imidazole [kg]	0.007
Methanol [kg]	0.016
NaOH [kg]	0.003
Water, completely softened [kg]	0.171
Water, cooling, unspecified [m^3]	0.0015
Energy and processing requirements	
Heat, unspecific, at chemical plant (boil-off solvents) [MJ]	0.305
Electricity [kWh]	0.022
Heat, natural gas [MJ]	0.020
Heat, other than natural gas [MJ]	0.007
Steam in chemical industry [kg]	0.002
Transport requirements	
Freight rail transport [tkm]	0.330
Lorry >16t [tkm]	0.055
Infrastructure requirements	
Chemical plant [unit]	1.34E-11
Waste and emissions	
Water, emissions to air [m^3]	0.0006
Water, emissions to water [m^3]	0.0009
Waste mixed plastics, inefficiencies [kg]	0.0008
Disposal of anion exchange membrane to incineration [kg]	0.0335

S1.2.5 Manufacture of the gas diffusion layer

Wang et al. (2020) use a carbon paper (CP) gas diffusion layer (GDL) with a microporous layer (MPL) manufactured by Fuel Cell Store under the product name of Freudenberg H14CP. CP is composed of hot pressed and carbonised carbon fibres with phenolic resin, and the MPL is usually composed of carbon black powder and PTFE (Duclos et al., 2017).

The material requirements of the CP were based on Hung et al. (2015), with a concentration of phenolic resin of 15% wt. The material requirements of the MPL were based on Park et al. (2008), with a carbon loading of 2 mg cm^{-2} and PTFE content of 20% wt. The carbon fibre weight was modified to match the area weight of 100 $g \cdot m^{-2}$ specified for Freudenberg H14CP in its technical datasheet. The organic solvents used in manufacture were not modelled. No pre-treatment losses were considered.

The energy requirements for the treatment and manufacture of the GDL are based on the work of Simons and Bauer (2015) and Evangelisti et al. (2017), using a thermoforming calendaring process as proxy. Transport requirements and infrastructure are identical to the inventory for the AEM since they are assumed to come from the same source. The disposal of the GDL is associated with waste of mixed plastics in landfill with approximately 15% water content. The detailed inventory is shown in Table S6.

Table S6. Inventory for the manufacture of the gas diffusion layer

Parameter	Amount
Functional unit output	
Gas diffusion layer, at plant [m^2]	1
Material requirements	
Carbon fibre [kg]	0.06
Phenolic resin [kg]	0.015
Carbon black [kg]	0.02
PTFE [kg]	0.005
Energy and processing requirements	
Heat, steam [MJ]	0.085
Heat, natural gas, at industrial furnace >100kW [MJ]	0.169
Electricity, grid [MJ]	3.58
Heat, heavy fuel oil, at industrial furnace 1MW [MJ]	0.222
Transport requirements	
Freight rail transport [tkm]	0.06
Lorry >16t [tkm]	0.01
Infrastructure requirements	
Chemical plant [unit]	4.0E-11
Waste and emissions	
Waste mixed plastics [kg]	0.012

The process for carbon fibre production was extracted from the Data on Production of Chemicals created for the EU Product Environmental Footprint (Wernet et al., 2017) and shown in Table S7. There are no assigned transport requirements since the process is assumed to happen on-site along with the GDL.

Table S7. Inventory for the production of carbon fibre

Parameter	Amount
Functional unit output	
Carbon fibre production, AU tech mix, at plant [kg]	1
Material requirements	
Argon, liquid [kg]	0.01
Lubricating oil [kg]	0.0002
water, completely softened, from decarbonised water, at user [kg]	0.057
water, decarbonised, at user [kg]	1.902
Acrylic fibre [kg]	2.08
Energy and processing requirements	
Heat, district or industrial, natural gas [MJ]	15.37
Natural gas, at consumer [kg]	0.37
Electricity, grid [kWh]	20.20
Heat, unspecific [MJ]	45.58
Infrastructure requirements	
Chemical plant [unit]	4.00E-10
Gas power plant [unit]	5.29E-10
Heat power cogeneration unit 1MW, electric+heat [unit]	3.28E-09
Heat power cogeneration unit 1MW, electric only [unit]	3.28E-09
Heat power cogeneration unit 1MW, heat only [unit]	3.28E-09
Heat power cogeneration unit 200kW, electric+heat [unit]	8.01E-09
Heat power cogeneration unit 200kW, electric only [unit]	8.01E-09
Heat power cogeneration unit 200kW, heat only [unit]	8.01E-09
Heat power cogeneration unit 500kW, electric+heat [unit]	2.72E-09
Heat power cogeneration unit 500kW, electric only [unit]	2.72E-09
Heat power cogeneration unit 500kW, heat only [unit]	2.72E-09
Industrial furnace, natural gas [unit]	3.84E-09
Waste and emissions	
Residue from cooling tower [kg]	9.51E-06
Waste mineral oil [kg]	0.0002

The acrylic fibre production process was extracted directly from the LCA by Yacout et al. (2016) and shown in Table S8. There are no assigned transport requirements since the process is assumed to happen on-site along with the carbon fibre and GDL.

Table S8. Inventory for the production of acrylic fibre

Parameter	Amount
Functional unit output	
Acrlyic fibre [kg]	1
Material requirements	
Acrylonitrile [kg]	0.91
Vinyl acetate [kg]	0.09
Sodium chlorate [kg]	0.006
Sodium metabisulfite [kg]	0.018
Sulfuric acid [kg]	0.0003
Sodium hydroxide (50%) [kg]	0.019
Titanium dioxide [kg]	0.0042
Sodium sulfate [kg]	0.007
Nitric acid [kg]	0.0024
Demineralized water [kg]	143.57
Energy and processing requirements	
Electricity, grid [kWh]	1.32
Steam [kg]	9.8
Infrastructure requirements	
Chemical plant [unit]	4.0E-10
Waste and emissions	
Waste effluent [m^3]	0.069
Hazardous waste from process [kg]	0.001
Chemical sludge [kg]	0.0012
Reused mixed plastics containers [kg]	0.0010

S1.2.6 Manufacture of electrolyte

The electrolyte used in the flow cell electrolyser is 1 M potassium hydroxide (KOH). The material requirements are a simple calculation of its components. Energy requirements for stirring are neglected. The deionization of water and the salt dissolution were assumed to be performed on-site at the electrolyser plant, thus no infrastructure requirements were assigned to this process. The waste and emissions are 95% of the water disposed of as waste water and waste treatment of sludge, using the disposal of sludge from NaCl electrolysis as proxy. The inventory is shown in Table S9.

Table S9. Inventory for the production of KOH 1M electrolyte

Parameter	Amount
Functional unit output	
KOH electrolyte 1M [kg]	1
Material requirements	
Potassium hydroxide [kg]	0.05
Water, completely softened [kg]	0.95
Transport requirements	
Freight rail transport [tkm]	0.60
Lorry >16t [tkm]	0.10
Waste and emissions	
Waste treatment, sludge from electrolysis [kg]	0.06
Water [kg]	0.94

S1.3 **Direct air capture system**

The direct air capture (DAC) process modelled is based on the process described by Keith et al. (2018) and analysed by Liu et al. (2020). Whilst still a conceptual design, all performance estimates are based on commercially available equipment, a proven process at a smaller-scale Carbon Engineering pilot plant, iterative prototypes developed by Royal HaskoningDHV, and comprehensive techno-economic analyses (Keith et al., 2018). Actual scale-up could still bring improvements or negative changes to the performance estimates.

The material requirements for the DAC plant are calculated from the initial chemicals needed to start the process in the plant. The land area associated with the plant is calculated from the quoted dimensions in an earlier publication by Holmes and Keith (2012): 0.016 km^2/Mt CO_2·year. However, the actual land use would be higher given those are only corresponding to the packings (Viebahn et al., 2019). Therefore, we assumed a two-fold increase in total land use. The cryogenic air separation unit in the original plant is not considered in the assessment because, unlike the oxy-fired calciner, the electric calciner does not need oxygen. The embodied emissions in the construction and decommissioning of the DAC plant are taken into account in the same way as in Liu et al. (2020), disregarding those of the equipment not needed in this model. They are modelled as direct CO_2 emissions in the inventory. The inventory for the DAC plant is presented in Table S11.

Table S10. Inventory for the Direct Air Capture plant

Parameter	Amount
Functional unit output	
DAC plant [unit]	1
Material requirements	
Potassium hydroxide [kg]	9.96E+05
Potassium carbonate [kg]	1.23E+06
Water, completely softened [kg]	1.78E+07
Calcium hydroxide (KOH as proxy) [kg]	1.10E+05
Infrastructure requirements	
Occupation, construction site [m^2a]	48,980
Occupation, industrial area [m^2a]	979,592
Transformation, from unknown [m^2]	48,980
Transformation, to industrial area [m^2]	48,980
Waste and emissions	
CO2-e emissions (construction & decommissioning) [kg]	2.13E+08

The inventory for the process of captured CO_2 as product was developed considering all make-up flows and losses. The inefficiencies in the captured and supplied CO_2 are considered as emissions back to the atmosphere. The plant design includes compression and clean-up of the product CO_2 from atmospheric pressure up to 150 bar. Although the ECCR operates at atmospheric pressure and would not need such high compression, it would still need to be scrubbed and dehydrated. Therefore, half of the power requirements associated with this subprocess are maintained in the model. This assumption is very conservative as it may overestimate the electricity required to provide the captured CO_2. Its inventory is presented in Table S12.

Table S11. Inventory of captured CO2 from Direct Air Capture

Parameter	Amount
Functional unit output	
Captured CO_2, DAC [kg]	1
Material requirements	
Carbon dioxide, in air [kg]	1.37
Potassium hydroxide [kg]	2.15E-04
Water, completely softened [kg]	4.162
Calcium carbonate [kg]	0.027
Energy and processing requirements	
Electricity [kWh]	0.244
Infrastructure requirements	
DAC plant [unit]	4.47E-11
Waste and emissions	
Carbon dioxide, air [kg]	0.37
Potassium hydroxide, air (NaOH as proxy) [kg]	2.15E-04
Calcium carbonate, waterborne disposal [kg]	0.027

S1.4 Adsorption system

The adsorbent selected for the adsorption bed is activated carbon (AC) (type BPL, 6/ 16 mesh, manufactured by the Pittsburgh Chemical Company) owing to the results of Zandvoort et al. (2020) in comparing cation zeolites and AC for various C_2H_4/CO_2 ratios. The design of the bed (namely, length/diameter ratio and thickness) is based on the experiments of Casas et al. (2012), scaled to match the required volume.

The adsorption system comprises two packed beds and the required total AC adsorbent in the lifetime of the system. The lifetime of each packed adsorption bed was assumed 20 years and of AC, 5 years, as estimated in Beccali et al. (2014). The material requirements are assumed to be stainless steel (Grade 304) for the case of the packed bed and plates. Energy requirements are included in the material extraction and manufacturing processes, and an estimated amount of electricity for welding based on the design of the bed.

The infrastructure requirements involve the factory, equipment, and land use needed to house the entire system. In order to estimate these values, the requirements for the ecoinvent process for an *Air separation facility* were used as a base, with the size scaled to the specific output of the adsorption system. The transport requirements to bring all the materials to a remote location were based on the distance from Brisbane to Dalby, first through freight rail to Toowoomba and then on a >32t lorry to Dalby. The wastes and emissions are the disposal of AC and steel at the end of lifetime of the AC and the complete facilities. The detailed inventory is shown in Table S13.

Table S12. Inventory for the adsorption system

Parameter	Amount
Functional unit output	
Adsorption system [unit]	1
Material requirements	
Activated carbon [t]	518.72
Stainless steel [t]	33.45
Stainless steel manufacturing [t]	33.45
Infrastructure requirements	
Occupation, construction site [m^2a]	329
Occupation, industrial area [m2a]	6577
Transformation, from unknown [m^2]	329
Transformation, to industrial area [m^2]	329
Aluminium, wrought alloy [kg]	3288
Chemical factory [kg]	29,595
Energy and processing requirements	
Electricity, welding [kWh]	0.47
Transport requirements	
Freight rail transport [tkm]	55,217
Lorry >32t [tkm]	44,174
Waste and emissions	
Carbon (disposal of AC) [t]	518.72
Disposal of steel to landfill [t]	33.45
Decommissioned chemical production facilities [kg]	29,595

S1.5 **Ethanol production by ECCR system**

This process comprises the entire production of 1kg of ethanol at 95% m/m through the electrocatalytic reduction of captured CO_2 obtained through direct air capture (DAC), and subsequent separation in the distillation system. Ethylene is a co-product separated through the adsorption system. The co-production is solved through system expansion by substitution, modelling ethylene production through ethane cracking, being the traditional benchmark.

The specific process used for ethylene production is an AusLCI inventory created on data provided by Qenos for their Botany Bay plant in New South Wales (NSW). The effect of the credit of the ethylene co-production is significant in the associated impact of the system. The validity for this particular assessment stands from a geographic perspective, as it is the current method to produce ethylene in an olefines production plant in the area of study. An LCA with a wider scope could incorporate the effect of cleaner energy or innovative processes for ethylene production. This may have an effect in the ultimate environmental impact of the proposed system.

The material requirements include the captured CO_2 (with its associated emissions and energy requirements), extra water for the electrolysis reaction and to maintain a constant volume of electrolyte, and the infrastructure requirements for the electrolyser stack, adsorption system, and distillation system. Make-up cooling water is required while the blowdown of the cooling tower is sent to wastewater treatment. The energy requirements include all electricity needed for each of the three systems. Details of their calculation can be found in their corresponding section. The thermal energy required is provided by an electric boiler with an assumed 95% efficiency. The total electricity requirement is met by medium voltage electricity from the different electricity grid scenarios.

All other transport and infrastructure requirements and wastes are implicit in the inventory of the subprocesses or materials. The infrastructure requirements for the distillation system use the ecoinvent process *Ethanol fermentation plant* as a proxy, assuming 60% of the entire plant to consider only the distillation columns needed. This assumption may be conservative considering fermenters usually involve the highest equipment and land component of the plant. The detailed inventory is presented in Table S14.

Table S13. Inventory of ethanol production via the ECCR system

Parameter	Amount
Functional unit output	
Ethanol production, by ECCR system [kg]	1
Co-production output (avoided products)	
Ethylene, at plant [kg]	0.416
Material requirements	
Captured CO_2 [kg]	3.123
Water, completely softened [kg]	2.028
Cooling water [m^3]	8.51E-04
Infrastructure requirements	
Electrolyser stack [unit]	7.91E-10
Adsorption system [unit]	7.91E-10
Distillation system [unit]	5.00E-10
Energy and processing requirements	
Electricity, ethylene separation (adsorption system) [kWh]	0.455
Electricity, compression (pre-adsorption recirculation) [kWh]	0.555
Heat, steam (distillation system) [MJ]	3.416
Electricity, cooling water (distillation system) [kWh]	0.003
Electricity, air cooling (distillation system) [kWh]	0.004
Electricity, compressors + pumps (distillation system) [kWh]	0.207
Electricity (electrolyser) [kWh]	27.066
Electricity (electrolyte pumps) [kWh]	0.879
Waste and emissions	
Water to wastewater treatment [m^3]	1.70E-04

S1.6 Ethanol production by bioethanol benchmark system

The largest producer of bioethanol in Queensland is Dalby Biorefinery, producing approximately 76 ML/a of bioethanol by the fermentation of red sorghum grain (Farrell and Santella, 2019). The bioethanol benchmark process in the LCA is based on a plant with the same size, output, and feedstock.

The AusLCI database has an unallocated process for ethanol and DDGS production based on data collected and estimated for a plant similar to Dalby Biorefinery. Modifications were done to adjust the performance to specifications in newer publications (Queensland Government, 2017) and personal communication (Sharp, 2020). Particular subprocesses were also adjusted to more closely reflect the geography of Dalby Biorefinery. Finally, other material requirements and wastes were complemented from ecoinvent processes for bioethanol production from wheat and sweet sorghum, adapting to the specific process and composition of red sorghum. Sorghum as a crop is modelled with high resolution in the AusLCI database, as a special inventory developed by CSIRO, the Department of Primary Industries NSW and Lifecycles for the AusLCI database (Australian Life Cycle Assessment Society, 2020).

The conversion of sorghum to ethanol was modelled as 2.5 kg sorghum/kg ethanol, as specified in a plant report (Queensland Government, 2017). Using the estimate in AusLCI of 0.282 kg DDGS/kg sorghum, the yield of DDGS is 0.892 kg DDGS/kg ethanol. Water requirements were based on the AusLCI and ecoinvent processes, and they are consistent with the range provided by first-hand information and specified in the same report (Queensland Government, 2017). Yeast is not included as

a material requirement since it is assumed to be recovered and propagated for consecutive fermentations. Material and energy requirements and waste treatments associated with yeast harvesting and propagation are not considered.

Soybean meal and cottonseed meal were used to solve the multifunctionality of the unallocated reference process through system expansion by substitution. The inventory of soybean meal was taken from the ecoinvent 3.5 database (Wernet et al., 2016). The inventory of cottonseed meal was taken from the AusLCI database (Edge Environment and Lifecycles, 2016), which was specifically compiled in detail by Grant et al. (2014) for the Rural Industries Research and Development Corporation of the Australian Government. Both processes are by-products, obtained through the main process of extracting oil from each respective crop. The used quantity for each scenario was calculated proportionally according to the protein content shown in Table 4.

The energy requirements are based on the energy consumption specified in the plant report (Queensland Government, 2017), differentiated between thermal and electrical energy according to the proportional spread in the AusLCI process. The thermal and electric energy requirements specific to dehydration (1 MJ and 0.0088 kWh per kg of ethanol, respectively) were removed in order to produce the functional unit at the same purity (95% m/m).

The infrastructure requirements are the ethanol fermentation plant itself, based on the total production of ethanol by the plant in the estimated 20 years of operational lifetime. The land use and occupation was calculated by measuring the area around Dalby Biorefinery in satellite photography (Google, n.d.). No construction or land transformation was considered. Transport requirements are based on the transport of sorghum from farm to plant and on the transport of natural gas in a pipeline to Dalby Biorefinery. Dalby uses a natural gas steam boiler to provide its heating requirements. The gas is obtained via the Dalby Gas Pipeline, an 8.9 km connection from the Dalby Compressor Station in the 438 km Roma to Brisbane gas pipeline (United Petroleum, n.d.). Only half of the distance of the main gas pipeline is considered, given that the Dalby Gas Pipeline is roughly at the middle of it. CO_2 emissions represent only the stoichiometric emission of biogenic CO_2: two moles of ethanol and two of CO_2 per mole of glucose. All other requirements and wastes are based on the ecoinvent and AusLCI referenced processes. The inventory is shown in Table S15. Note only one co-production substitute output is used per scenario, not both of them in the same inventory.

Table S14. Inventory of bioethanol production via sorghum fermentation

Parameter	Amount
Functional unit output	
Ethanol from sorghum, QLD [kg]	1
Co-production output	
- *Soybean meal (substitute for DDGS) [kg]* ***or***	0.555
- *Cottonseed meal (substitute for DDGS) [kg]*	0.648
Material requirements	
Sorghum grain, Western Downs and NW slopes and plains [kg]	1.055
Sorghum grain, northern zone NSW [kg]	1.055
Sorghum grain, Darling Downs, QLD [kg]	1.055
Lubricating oil [kg]	2.31E-04
Water, Darling Downs [kg]	7.296
Water, completely softened [kg]	0.015
Chlorine, liquid [kg]	6.43E-06
Sodium chloride, powder [kg]	8.03E-05
Sulfuric acid [kg]	0.027
Energy and processing requirements	
Heat, natural gas, at industrial furnace [MJ]	9.482
Electricity, QLD	0.334
Infrastructure requirements	
Occupation, industrial area [m2a]	0.087
Ethanol fermentation plant [unit]	8.33E-10
Transport requirements	
Truck, 40t [tkm]	0.633
Pipeline, natural gas [tkm]	0.036
Waste and emissions	
Carbon dioxide, biogenic [kg]	0.955
Disposal, solid waste [kg]	6.43E-05
Disposal, used mineral oil [kg]	6.43E-05
Water to wastewater treatment [m^3]	1.54E-05

S1.7 **High and medium voltage electricity**

The generation of high voltage and medium voltage electricity was modelled taking the corresponding AusLCI process as base, changing the electricity grid mix for each scenario. All emissions, infrastructure, and energy losses are considered. The inventory of high voltage generation and medium voltage is found in Table S16 and S17, respectively.

Table S15. Inventory for high voltage electricity generation

Parameter	Amount
Functional unit output	
Electricity, high voltage (High, Mid, Low) [kWh]	1
Energy and processing requirements	
Electricity grid mix (High, Mid, Low) [kWh]	1.045
Infrastructure requirements	
Transmission network, high voltage [km]	8.44E-09
Transmission network, long distance [km]	3.17E-10
Waste and emissions	
Ozone [kg]	4.50E-06
Dinitrogen monoxide [kg]	5.00E-06
Energy losses in electricity transmission [kWh]	0.045

Table S16. Inventory for medium voltage electricity generation

Parameter	Amount
Functional unit output	
Electricity, medium voltage (High, Mid, Low) [kWh]	1
Material requirements	
Sulfur hexafluoride, liquid [kg]	1.29E-07
Energy and processing requirements	
Electricity, high voltage (High, Mid, Low) [kWh]	1
Electricity, high voltage (High, Mid, Low) (voltage transformation loss) [kWh]	4.60E-03
Electricity, medium voltage (High, Mid, Low) (transmission loss) [kWh]	2.70E-03
Infrastructure requirements	
Transmission network, medium voltage [km]	1.86E-08
Waste and emissions	
Sulfur hexafluoride, to air [kg]	1.29E-07
Energy losses in electricity transmission [kWh]	7.30E-03

S2. Process modelling description

S2.1 Electrolyser model and rigorous carbonate equilibria

The electrolyser design is based on the experiment of Wang et al. (2020), using its innovative catalyst for the CO_2 reduction reaction (CO_2RR) coupled with a gas diffusion layer (GDL). As first developed in a flow cell reactor by Dinh et al. (2018), the GDL prevents the CO_2 from converting to bicarbonate by only allowing a short diffusion distance between the layer and the catalyst. Tan et al. (2020) demonstrated that the local concentration of CO_2 in the active spaces of the catalyst is the main factor in producing C2 hydrocarbons at high current densities. The GDL is able to promote a higher concentration of CO_2 available for reaction.

Table S18 summarises pertinent characteristics and performance of the electrolyser. For simplicity of analysis and separation, only ethanol, ethylene, and hydrogen were assumed to be produced, disregarding the presence of marginal products. The Faradaic efficiency (FE) of ethanol and ethylene was taken as the reported average plus its standard deviation, with the remainder assigned to hydrogen. The exact FE of every product can be found in the original report (Wang et al., 2020).

Table S17. Characteristics of electrolyser

Parameter	Amount
Operating conditions	
Temperature [°C]	25
Pressure [atm]	1
Faradaic efficiencies	
Ethanol [%]	53
Ethylene [%]	38
Hydrogen [%]	9
KOH electrolyte concentration [M]	1
Current density [mA/cm^2]	300
Cathode	
Material	34% N/C-Cu
E_{CO2RR} [V vs RHE]	-0.68
Energy efficiency [%]	31.6
Anode	
Material	Ni foam
Full cell efficiency [%]	26.2

Partial current densities are calculated from the FE of each reported product i and the total current density (j_T).

$$j_i = j_T \cdot FE_i$$

The molar flowrates (Q_i) of each product can be calculated with the electrode area (A), the Faraday constant (F), and the number of electrons in each reaction (α_i).

$$Q_i = \frac{j_i \cdot A}{F \cdot \alpha_i}$$

The rate of reaction or consumption of CO_2 can then be derived from the molar flowrates and the stoichiometric coefficient (z) of CO_2 in the reaction of each product.

$$CO_{RX} = \sum Q_i \cdot z_i$$

At steady-state, the flowrate of unreacted CO_2 leaving the gas chamber is the difference between the inlet CO_2 flowrate and the CO_2 consumption reaction rate.

The main reactions occurring in both cathode and anode with their standard electrode potential at 298K are presented in Table S19.

Table S18. Main reactions in system

	Half-cell electrochemical reactions	Potential (V vs RHE)[a]
Cathode	$2CO_2 + 9H_2O + 12e^- \rightarrow CH_3CH_2OH + 12OH^-$	0.09
	$2CO_2 + 8H_2O + 12e^- \rightarrow CH_2CH_2 + 12OH^-$	0.08
	$2H_2O + 2e^- \rightarrow H_2 + 2OH^-$	0.00
Anode	$4OH^- \rightarrow O_2 + H_2O + 4e^-$	1.23

[a]Hori (2008)

By defining the FE of ethanol, ethylene, and hydrogen as x, y, and 1 – (x+y), respectively, the global reaction can be written as,

$$2(x+y)CO_2 + (6-3x-4y)H_2O \rightarrow xCH_3CH_2OH + yCH_2CH_2 + (1-x-y)6H_2 + 3O_2$$

The rate of reaction of each product can then be obtained through the rate of consumption of CO_2 and the stoichiometric coefficient of the global reaction. The gaseous flowrate leaving the gas chamber of the electrolyser will be the flowrate of unreacted CO_2 plus the rates of reaction of ethylene and hydrogen. The electrolyte is recirculated through the cathode and anode, respectively. At steady-state, a specific composition is maintained and a reduced flowrate is continuously sent to the distillation unit.

Oxygen produced in the anode is vented through the recirculation of the anolyte in the pumping system. While there would be gaseous CO_2 in the anode as well, the model assumes only oxygen is vented and there are no CO_2 losses. The crossover of ethanol from cathode to anode is negligible with an anion exchange membrane (Ma et al., 2020). Therefore, all the ethanol is assumed to stay in the catholyte and arrive to the distillation system to be separated. However, all ions and CO_2 are expected to crossover through the membrane. Therefore, the recirculated electrolyte coming back from the distillation system that is pumped to the cathode is expected to reach equilibrium with the anolyte through the membrane. This ensures maintaining all necessary species required for the reactions in each chamber.

A rigorous carbonate equilibria calculation is required to know the composition of the electrolyte that will be pumped to the distillation unit. CO_2 coming from the gaseous inlet to the gas chamber and crossing the GDL will continuously dissolve in the electrolyte. To determine the concentration of CO_2 and other carbonate species at steady-state, an equilibrium-based model was developed. The carbonate equilibria are defined by the following reactions.

$$CO_{2(g)} + H_2O \leftrightarrow CO_{2(aq)} + H_2O \quad \ldots (S1)$$

$$CO_{2(aq)} + H_2O \leftrightarrow H_2CO_3 \quad \ldots (S2)$$

$$H_2CO_3 \leftrightarrow H^+ + HCO_3^- \quad \ldots (S3)$$

$$HCO_3^- \leftrightarrow H^+ + CO_3^{2-} \quad \ldots (S4)$$

According to Henry's law, the concentration of dissolved CO_2 can be obtained by the partial pressure of CO_2 in the system.

$$K_0 = \frac{[CO_{2(aq)}]}{P_{CO_2}} \quad \ldots (S5)$$

Given the equilibrium of reaction S2 substantially favours the production of $CO_{2(aq)}$, the equilibrium constant of the protolysis and of the hydration reaction of H_2CO_3 is usually reported as a composite constant K_1 for the joint carbonate species $H_2CO_3^*$ or $CO_2^*{}_{(aq)}$. The concentrations of $CO_{2(aq)}$ and $CO_2^*{}_{(aq)}$ are almost identical and the composite constant K_1 is reported from experimental determination with higher accuracy (Stumm and Morgan, 1995). This species is generally accepted as the active species for the CO_2RR (Zhong et al., 2015).

The equilibrium constants are then defined as

$$K_1 = \frac{[H^+][HCO_3^-]}{[CO^*_{2(aq)}]} \quad \dots \text{(S6)}$$

$$K_2 = \frac{[H^+][CO_3^{2-}]}{[HCO_3^-]} \quad \dots \text{(S7)}$$

The values of these equilibrium constants can be calculated in function of temperature according to the parameters shown in Table S20.

Table S19. Carbonate equilibria parameters in function of temperature (T)

pK_0	-2385.73/T – 0.0152642T + 14.0184	(Harned and Davis, 1943)
pK_1	3404.71/T + 0.032786T – 14.8435	(Harned and Davis, 1943)
pK_2	2902.39/T + 0.02379T – 6.4980	(Harned and Scholes, 1941)
ln K_W	148.9802 – 13847.26/T – 23.6521·log(T)	(Millero, 1995)

Calculating K_0 at ambient conditions, the maximum concentration of dissolved CO_2 in water is 0.0338M. However, the CO_2 solubility in an electrolyte is decreased by the presence of ions in a phenomenon called the "salting-out" effect. Its effect can be quantified by the Sechenov equation:

$$\log\left(\frac{[CO_2]_{Henry}}{[CO_2]_E}\right) = K_S \cdot C_E$$

where $[CO_2]_{Henry}$ is the CO_2 solubility in pure water, $[CO_2]_E$ the solubility in the electrolyte, and K_S the Sechenov constant, which is given by the following relation.

$$K_S = \sum (h_i + h_{CO_2}) n_i$$

where h_i and h_{CO2} are the ion and gas-specific parameters for ion *i* and of CO_2, respectively, and n_i is the index of ion *i* in the formula of the salt. Given that, at steady-state, the equilibrium will convert the KOH electrolyte in $KHCO_3$ because of the continuous input of gaseous CO_2 (Blom et al., 2019), the parameters corresponding to a $KHCO_3$ electrolyte at 298K were taken from Weisenberger and Schumpe (1996) and are shown in Table S21.

Table S20. Sechenov equation parameters

h_{K^+}	0.0922 $m^3 \cdot kmol^{-1}$
h_{HCO3^-}	0.0967 $m^3 \cdot kmol^{-1}$
h_{CO2}	-0.0172 $m^3 \cdot kmol^{-1}$

Therefore, the maximum concentration of $CO_2^*{}_{(aq)}$ in the electrolyte is 0.0237 M.

By knowing the value of $[CO_2^*{}_{(aq)}]$, and adding the concentration condition,

$$C_T = \left[CO^*_{2(aq)}\right] + \left[HCO_3^-\right] + \left[CO_3^{2-}\right] \quad \ldots (S8)$$

the ion charge balance,

$$[H^+] + [K^+] = [OH^-] + [HCO_3^-] + 2[CO_3^{2-}] \quad \ldots (S9)$$

and the dissociation of water,

$$K_w = [H^+][OH^-] \quad \ldots (S10)$$

the system of equations (Equations S6 – S10) can be solved for $[H^+]$. The concentration of all species can then be obtained, which will be the composition of the stream sent to distillation.

The power requirements of the electrolyser include the electricity required for the cell and the pumps to recirculate the electrolyte. The full cell potential (E_{cell}) is the sum of the potential of the CO_2RR, the oxygen evolution reaction (OER) and the overpotential of the OER. Given the overpotential for OER in Wang et al. (2020) was not specifically measured, an overpotential of 0.4 V was used according to the experiments on Ni foam electrodes by Liang et al. (2015). The power requirements (*P*) are then,

$$P = E_{cell} \cdot A \cdot j_T$$

The power requirements for the pumps were determined by the required head, the total volumetric flow of electrolyte, and an efficiency of 75% to maintain a conservative value.

The following additional assumptions were considered:

- The ideal gas law holds due to the operation at atmospheric pressure
- No significant change in temperature between inputs and outputs of electrolyser due to the flow cell system
- The electrolyte recirculation was scaled-up linearly from the original design in the absence of any better information
- The inlet gas flowrate was scaled-up linearly from the original design in the absence of any better information
- The electrolyser operates at a balanced pressure in anode and cathode
- No change in performance due to fouling on either electrode
- No variations in feed
- Start-up/shutdown is instantaneous

Wang et al. (2020) performed a stability test with a membrane electrode assembly to identify the integrity of the catalyst. After 15 hours, no drop on the performance was recorded. In this model, the maximum concentration of ethanol attainable in the electrolyte was determined by an assumed 10,000-minute period of continuous operation with the same electrolyte. At steady-state, this concentration is maintained in the electrolyte and the stream that is sent for separation to the distillation unit. While this period is longer than the test of Wang et al. (2020), it allows building up a higher concentration of ethanol to make the separation in the distillation system more efficient. This assumption is highly conservative considering the lifetime of continuous operation in current alkaline electrolysers (Bertuccioli et al., 2014). However, experiments have not concluded that this is the maximum operation period with the same recirculated electrolyte. Further experimentation with this electrolyser is needed to test the limits of its performance and determine the maximum operation period with the same recirculated electrolyte.

S2.2 Adsorption model for C_2H_4/CO_2 separation

The separation of ethylene (C_2H_4) from the gaseous products is accomplished with a simplified vacuum swing adsorption (VSA) model using activated carbon (AC) based on the work of Zandvoort et al. (2020) and Maring and Webley (2013). The adsorption unit consists of a dual bed packed with AC and a system of valves that allow separating the C_2H_4 in high purity from the CO_2 and hydrogen (H_2) by a pressure swing range between 2 bara and 0.2 bara. The rigorous calculation of recovery, heat exchanger requirements and exact breakthroughs are beyond the scope of this work.

The stream is modelled as a binary mixture given H_2 is not adsorbed in AC. However, the mass balance still accounts for the fraction of H_2 in the mix. The adsorption isotherms were calculated through the dual-site Langmuir model, described by the following expression:

$$q = q_{A,sat}\frac{b_A p}{1 + b_A p} + q_{B,sat}\frac{b_B p}{1 + b_B p}$$

With parameters b_A *and* b_B in function of temperature (T)

$$b_A = b_{A0}e^{\frac{E_A}{RT}};\ b_B = b_{B0}e^{\frac{E_B}{RT}}$$

The parameter fits were taken from Zandvoort et al. (2020), which were fitted through the experimental data of Reich et al. (1980) for AC (BPL). The parameter fits can be found in Table S22.

Table S21. Dual-site Langmuir parameter fits for CO_2 and C_2H_4 in activated carbon

	Site A			**Site B**		
	n_A sat [mol/kg]	b_{A0} [Pa^{-1}]	E_A [kJ/mol]	n_B sat [[mol/kg]	b_{B0} [Pa^{-1}]	E_B [kJ/mol]
CO_2	3.5	5.62E-10	22.5	7.6	5.89E-11	22.6
C_2H_4	3.6	1.30E-09	24	4.4	9.63E-11	21.5

Table S23 indicates the conditions and properties of the bed according to the process.

Table S22. Properties of inlet stream and bed

Property	Amount
Temperature, T_{feed} [K]	298.15
High operating pressure, P_H [bar]	2.0
Low operating pressure, P_L [bar]	0.2
Fraction of ethylene, y_{C2H4}	0.04
Fraction of CO_2 y_{CO2}	0.95
Fraction of H_2, y_{H2}	0.01
Bed void, ε_{bed}	0.37[a]
Density, ρ_{bed} [kg/m^3]	480.5[a]
Total void fraction, ε_{total}	0.69[a]
Heat capacity, C_{AC} [J/kg·K]	1050[a]

[a] Maring and Webley (2013)

Knowing the adsorption capacity of the bed for each component is a function of its partial pressure and temperature, the difference between adsorption capacities between the high operating pressure (P_H) and low operating pressure (P_L) determines the working capacity (q) of the bed for each component. That amount will be desorbed alongside the gas in the void of the bed, which is the same composition as the adsorbed phase.

$$q_{C2H4} = f(P_{C2H4}, P_{CO2}, T) \quad ; \qquad q_{CO2} = f(P_{C2H4}, P_{CO2}, T)$$

$$q = f(P_H, P_L, T)$$

The mass of adsorbent was determined through the loading of ethylene in the bed, which follows the material balance,

$$q_{C2H4} = \frac{\dot{n}}{m_{ads}} \int_0^{t_{ss}} (y_{feed} - y_{exit}) dt$$

where $\dot{n}$ is the total molar flowrate entering the bed, m_{ads} is the mass of the adsorbent, and t_{ss} is the time till steady-state.

The total amount of each component in the bed are the moles adsorbed in the bed and the moles in the gas phase in the void,

$$n_i = q_i(P_i, P_j, T) \cdot m_{ads} + \frac{y_i PV}{RT}$$

Based on the Ideal Adsorbed Solution Theory (IAST) of Myers and Prausnitz (1965) and the transient breakthrough simulations and experiments of Zandvoort et al. (2020), the breakthrough of ethylene happens after that of CO_2. This suggests being able to recover CO_2 at high purity after its breakthrough ($t_{b,CO2}$) to be recirculated to the electrolyser before ethylene breaks through ($t_{b,C2H4}$). After saturation, the blowdown will desorb CO_2 more rapidly until trace amounts are only present in the exit gas, considered the time of depletion of CO_2 ($t_{d,CO2}$). At this point, the exit gas will have ethylene at high purity until the end of the blowdown cycle (t_c).

Figure S1 shows a schematic of the general stages in the cycle, indicating the pressure in each bed (in bar) and the open/closed valves in each configuration. Stream A comes from the electrolyser and contains a mix of 95.0% CO_2, 4.1% C_2H_4, and 0.9% H_2. Hydrogen is assumed to flow unaltered through the bed in its entirety. Therefore, at the Saturation stage, the first bed is saturated with CO_2 and C_2H_4, defined by the breakthrough of C_2H_4. At this point, the Equalisation stage starts by closing all valves except the one between beds and reaching an equilibrium pressure of 1.1 bar between them. The 1st Blowdown/Repressurisation stage starts by commencing the blowdown of the first bed through Stream B, which goes back to Stream A to be re-compressed and looped in the adsorption system. After the gas in the bed void blows down, CO_2 will be desorbed at a faster rate than the ethylene. This stream has an average composition of 97% CO_2 and 3% C_2H_4. This stream is recirculated to Stream A with all the ethylene desorbed with the CO_2 to be able to eventually separate it. Simultaneously, the second bed will now start adsorbing Stream A from the electrolyser and Stream B from the first bed, increasing its pressure. Stream C will first have H_2 flowing through without having been adsorbed, and then CO_2 too after its breakthrough. After all CO_2 is desorbed from the first bed, the 2nd Blowdown/Feed stage begins by opening the blowdown valve now to Stream D, which will be C_2H_4 in high purity. It will continue its blowdown until the breakthrough of C_2H_4 is reached in the second bed. At this point, the Saturation stage is reached again in its mirrored configuration in the second bed.

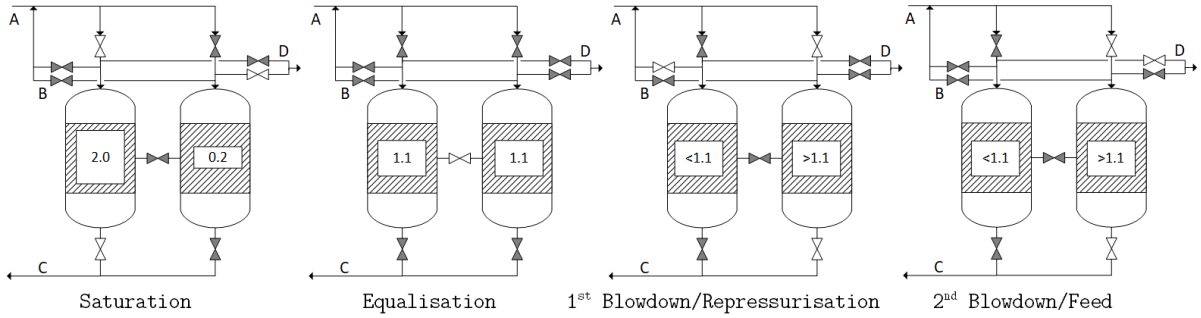

Figure S1. Schematic of adsorption cycles in dual-bed system

To determine the mass balance of the entire system at steady-state, several assumptions were made. The breakthrough times were re-calculated according to the working capacity of the bed, resulting in a cycle time at cyclic steady-state ($t_{c,SS}$) of 13.4 minutes. In this calculated cycle, the equalisation step is instantaneous. The trace amounts of hydrogen recirculated with the CO_2 were assumed to not have an effect on the performance of the electrolyser. In case it is indeed hindered by impurities in the inlet gas stream, these trace amounts of hydrogen in Stream C exiting the blowdown before $t_{d,CO2}$ may be combusted before being recycled to the gas chamber. The desorption of ethylene is linear and only in function of $t_{d,CO2}$ to calculate the composition of this stream. The mass balance of the entire system reflects this recirculated fraction. Finally, during blowdown, the gas in the void is assumed to leave in its entirety. The vacuum and blower work are calculated through isentropic compression assuming a constant isentropic efficiency of 75%. The bed is assumed to be adiabatic and isosteric heats are neglected.

$$W = \frac{1}{\eta}\frac{kRT_{in}}{k-1}\left[\left(\frac{P_{out}}{P_{in}}\right)^{\frac{k-1}{k}} - 1\right]$$

The ethylene separation to pure product is 88.1% with respect to the inlet gaseous stream, with the remainder continuously looped through the adsorption system. The recirculated Stream C is virtually 100% CO_2 to be used as feed to the electrolyser gas chamber. The trace amounts of products in the recirculation to the gas chamber are assumed to have no effect to the performance of the electrolyser. As hydrogen flows through the bed before the breakthrough of CO_2, a partial stream of hydrogen could be separated from the mixed stream. However, hydrogen is not considered a co-product in the inventory as it could overestimate the benefits of this theoretical and simplified adsorption model.

The gas exiting the gas chamber of the electrolyser has a low concentration of ethylene (0.3%) because of the large amount of unreacted CO_2. A recirculation loop was included at the exit of the gas chamber to increase the ethylene concentration of the stream that is sent to the adsorption system. As there is no data available for the performance of the electrolyser with products in the inlet gas stream to the gas chamber, the CO_2 concentration in the stream was assumed to be maintained at a minimum of 95%, allowing an ethylene concentration of 4.1% and 0.9% hydrogen. The compression work for this recirculation is low because it only has to overcome the pressure drop across the stack. However, it is included based on isentropic compression with an efficiency of 75% and is accounted in the energy requirements of the adsorption system.

S2.3 Distillation model and simulation

The distillation system separates the produced ethanol in the cathode from the electrolyte, which is a combination of water, carbonate and potassium ions, and CO_2 in dissolution. This cannot be achieved with a simple distillation column because of the CO_2 present, both in dissolution and in carbonate ions that can shift to CO_2 in the equilibria. Therefore, an innovative separation system was designed to ensure minimal losses while achieving the intended product, ethanol 95% m/m. The model was simulated in Aspen Plus, and a complete heat integration was developed to minimise the energy requirements of the plant. Note that the following description of the process already considers the final design modifications resulting from the heat integration.

Figure S2 presents a process flow diagram of the distillation unit simulation. The feed stream, coming directly from the bleed of the catholyte stream in the electrolyser cell, is preheated up to a temperature of 88°C. This stream is fed to the first stage of a stripping column with no condenser (T-01). The stripping column separates 99%mol of the ethanol from the liquid mixture through the overhead stream and removing through the bottoms 75% of the water and all of the carbonate ions in solution. The overheads stream of the stripper is compressed to 3.1 bar in a heat pump (C-01), increasing the temperature of the process vapour high enough to satisfy the heat requirements of the reboiler in the stripper (E-03). The now condensed process stream is cooled to 40°C by passing through the first heat exchanger (HEX) that preheats the feed (E-01). A flash drum (V-01) then allows CO_2 to leave as a gaseous stream (97.4% purity, 2 bar). The liquid fraction containing water and ethanol in stream 30 is assumed to be separated and the trace amounts of gaseous water and ethanol in the resulting stream are assumed negligible before being recirculated to the gas chamber of the electrolyser. The liquid is then divided and directed to the split pressure rectifier unit.

The split pressure rectifier is modelled in a similar configuration to the double-effect distillation and thermal integration by Palacios-Bereche et al. (2015). The unit comprises two columns, a low-pressure column (1.1 bar) and a high-pressure column (3.1 bar), which significantly reduce the energy requirements to operate them. By increasing the operating pressure of the high-pressure column (T-03), its condenser can thermodynamically satisfy the requirements of the reboiler of the low-pressure column (T-02). Because there are still considerable amounts of CO_2 in the top stream of the rectifiers, both columns have a three-way partial condenser, allowing a vapour bleed (79% ethanol, 17% CO_2, 4%

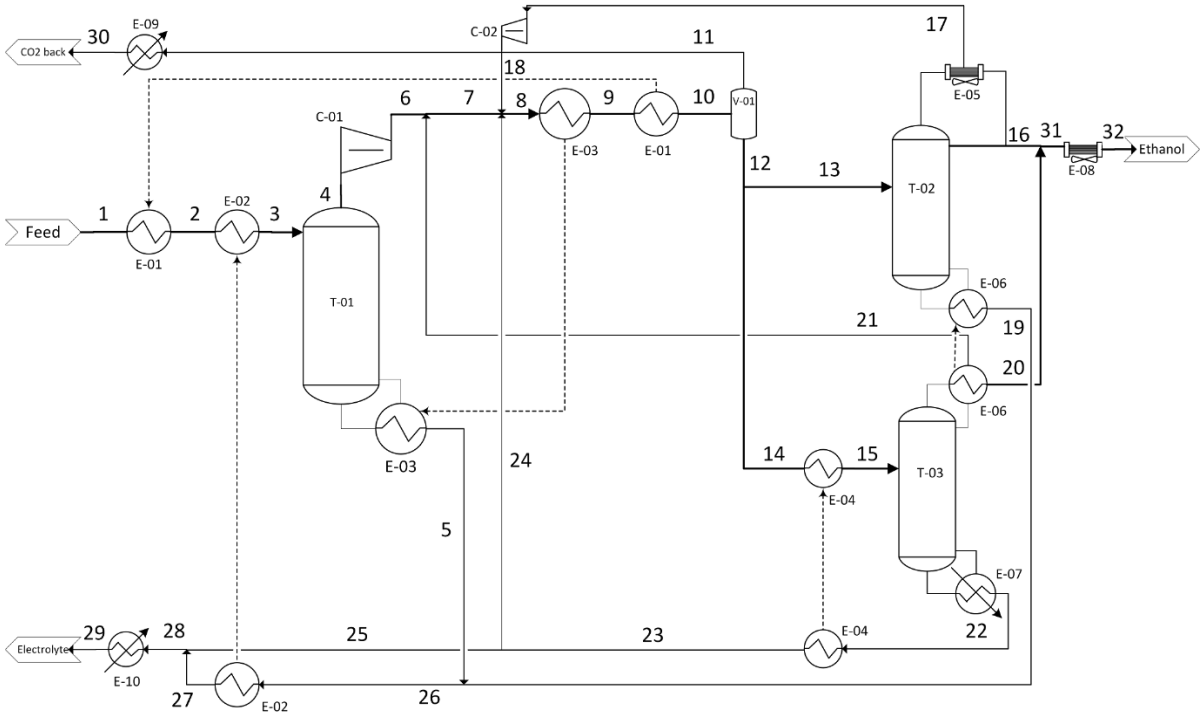

Figure S2. Process flow diagram of the distillation unit simulation

H_2O) to be compressed and returned to the process upstream of the stripper reboiler process HEX (E-03). This reduces the duty required and allows both columns to distil and deliver the ethanol product at the same composition.

The bottoms of T-02 (98% water, 2% ethanol) and the stripper T-01 (carbonate solution) are mixed and then cooled down by providing the heat requirements of the second HEX that preheats the feed (E-02). The bottoms water of T-03, after preheating its own feed to bubble point, split 18% of its flow to mix with the process upstream of E-03, along with the bleeds of the rectifiers. This brings the superheated vapour process stream after the heat pump to saturation, reducing significantly the required area of the condenser/reboiler HEX. The rest of the T-03 bottoms mixes with the stream of the other bottoms, and are then cooled down back to 30°C to go back to the ECCR pump system and be used as electrolyte.

The energy efficiency of the plant is 92% (considering the energy consumed and the low heating value of ethanol in the product and in the feed), with a net power input to the system of 9.17 MW. While the associated energy cost of operating the heat pump is considerable, the saving of heat duty is even greater. A coefficient of performance (CoP) of 8.57 is evidence of a good design to reduce energy requirements.

$$CoP = \frac{energy\ saved\ in\ stripper}{energy\ used\ in\ heat\ pump} = \frac{13.89\ MW}{1.62\ MW} = 8.57$$

The recovered CO_2 and electrolyte are suitable to be re-used in the ECCR system, reducing the material requirements to operate the overall system. The purification of ethanol as final product is 93%, with the remainder recycled in the electrolyte continuously. The recovery of CO_2 is 99.9%, with a marginal loss found in the ethanol product. Because of the shifts in the carbonate equilibria during the distillation,

36% of carbonate is converted to CO_2 and recovered in gas form to be recirculated and used in high purity form. Because of the removal of CO_2, the equilibria shift back towards a higher pH and increased carbonate ions. When mixed with necessary make-up water before entering the electrolyser once again, it has the same alkalinity and composition required to run in both cathode and anode.

For the simulation, a number of assumptions were considered for the system, using the values presented in Table S24. The minimum temperature of utility streams used were modelled considering geographical conditions. In the process HEX E-03 and E-06, one stream is boiling and the other is condensing. The minimum temperature approach of 5°C in these HEX is possible by using High Flux tubing, which has a high heat flux transfer area (Wisz et al., 1981). The thermo package used was previously configured for carbonate electrolyte with a reactive chemical absorption system (Harkin, 2012), including the electrolyte-NRTL model for mixed solvent electrolyte system (Chen and Song, 2004). The stripping column is then converged based on equilibrium.

Table S23. Overview of simulation assumption values

Property	Amount
Minimum temperature with cooling water	30°C
Minimum temperature with air cooling	50°C
Utility steam pressure	5 bar
Minimum temperature approach for utility and process heat exchangers	10°C
Minimum temperature approach for E-03 and E-06	5°C
Pressure drop in heat exchangers with liquid streams	0.7 bar
Pressure drop in heat exchangers with gaseous streams	0.3 bar
Isotropic efficiency of heat pump	72%

The recycling stream to be re-used as electrolyte (Stream 29) has 1.2% m/m of ethanol. To model the steady-state operation of the entire ECCR system, the electrolyser stack was re-scaled to produce the necessary amount of ethanol to arrive to the feed concentration of 15.2% m/m of ethanol considering the composition of the recycled electrolyte. More experimentation with the selected electrolyser might prove the performance is maintained for a longer period. This would allow a higher concentration of ethanol in the catholyte, increasing its composition in the feed stream to distillation and reducing the energy requirements of the system.

Table S25 is the full stream table for the converged steady-state Aspen Plus model.

Table S24. Full stream table of the converged distillation simulation model

Stream	1	2	3	4	5	6	7	8	9	10
Temperature [°C]	30.0	78.0	88.3	99.8	105.8	217.2	215.7	131.3	110.8	40.7
Pressure [bar]	2.6	1.9	1.2	1.1	1.2	3.1	3.1	3.1	2.8	2.1
Mass Vapor Fraction	0	0.001	0.005	1	0	1	1	1.000	0.075	0.038
Mass Liquid Fraction	1	0.999	0.995	0	1	0	0	0.000	0.925	0.962
Mass Enthalpy [J/kg]	-1.4E+07	-1.4E+07	-1.4E+07	-1.1E+07	-1.5E+07	-1.0E+07	-1.0E+07	-1.0E+07	-1.1E+07	-1.2E+0
Mass Flow [kg/s]	14.71	14.71	14.71	7.49	7.22	7.49	7.61	8.17	8.17	8.17
Mass Fractions										
H2O	0.755	0.755	0.756	0.664	0.865	0.664	0.654	0.669	0.669	0.669
CO2	0.001	0.002	0.003	0.040	0.000	0.040	0.041	0.039	0.039	0.039
H3O+	9.2E-10	3.3E-10	9.4E-11	0.0E+00	3.2E-12	0.0E+00	0.0E+00	1.1E-11	2.1E-07	6.1E-07
K+	0.036	0.036	0.036	0.000	0.073	0.000	0.000	0.000	0.000	0.000
OH-	6.4E-09	2.2E-07	1.2E-06	0.0E+00	2.8E-04	0.0E+00	0.0E+00	9.3E-14	2.9E-11	4.2E-13
HCO3-	0.056	0.055	0.051	0.000	0.006	0.000	0.000	0.000	0.000	0.000
CO3--	0.000	0.001	0.002	0.000	0.053	0.000	0.000	0.000	0.000	0.000
ETHANOL	0.152	0.152	0.152	0.296	0.003	0.296	0.305	0.292	0.292	0.292

Stream	11	12	13	14	15	16	17	18	19	20
Temperature [°C]	40.7	40.7	40.7	40.9	102.5	76.8	76.8	142.5	103.9	108.8
Pressure [bar]	2.1	2.1	2.1	5.0	4.3	1.1	1.1	3.1	2.6	3.1
Mass Vapor Fraction	1	0	0	0	0.001	0	1	1	0	0
Mass Liquid Fraction	0	1	1	1	0.999	1	0	0	1	1
Mass Enthalpy [J/kg]	-8.9E+06	-1.3E+07	-1.3E+07	-1.3E+07	-1.3E+07	-6.4E+06	-5.8E+06	-5.7E+06	-1.5E+07	-6.2E+06
Mass Flow [kg/s]	0.31	7.86	4.02	3.84	3.84	1.15	0.06	0.06	2.81	1.04
Mass Fractions										
H2O	0.013	0.695	0.695	0.695	0.695	0.050	0.019	0.019	0.975	0.050
CO2	0.973	0.003	0.003	0.003	0.003	0.000	0.167	0.167	0.000	0.000
H3O+	0.0E+00	6.3E-07	6.3E-07	6.3E-07	4.1E-07	5.9E-12	0.0E+00	0.0E+00	1.3E-08	3.7E-12
K+	0.000	0.000	0.000	0.000	0.000	0.000	0.000	0.000	0.000	0.000
OH-	0.0E+00	4.3E-13	4.3E-13	4.4E-13	1.3E-11	9.1E-17	0.0E+00	0.0E+00	1.2E-08	2.8E-16
HCO3-	0.000	0.000	0.000	0.000	0.000	0.000	0.000	0.000	0.000	0.000
CO3--	0.000	0.000	0.000	0.000	0.000	0.000	0.000	0.000	0.000	0.000
ETHANOL	0.014	0.303	0.303	0.303	0.303	0.950	0.814	0.814	0.025	0.950

Stream	21	22	23	24	25	26	27	28
Temperature [°C]	108.8	135.4	51.4	51.4	51.4	104.9	88.0	80.7
Pressure [bar]	3.1	3.3	2.6	3.5	2.6	2.6	1.9	1.9
Mass Vapor Fraction	1	0	0	0	0	0	0	0
Mass Liquid Fraction	0	1	1	1	1	1	1	1
Mass Enthalpy [J/kg]	-5.5E+06	-1.5E+07	-1.6E+07	-1.6E+07	-1.6E+07	-1.5E+07	-1.5E+07	-1.5E+07
Mass Flow [kg/s]	0.12	2.68	2.68	0.50	2.18	10.02	10.02	12.20
Mass Fractions								
H2O	0.021	0.975	0.975	0.975	0.975	0.895	0.896	0.910
CO2	0.089	0.000	0.000	0.000	0.000	0.000	0.000	0.000
H3O+	0.0E+00	2.2E-08	4.1E-09	4.1E-09	4.1E-09	3.0E-12	2.7E-12	2.4E-12
K+	0.000	0.000	0.000	0.000	0.000	0.053	0.053	0.043
OH-	0.0E+00	1.9E-08	3.6E-09	3.6E-09	3.6E-09	2.9E-04	1.7E-04	1.3E-04
HCO3-	0.000	0.000	0.000	0.000	0.000	0.004	0.004	0.003
CO3--	0.000	0.000	0.000	0.000	0.000	0.038	0.038	0.031
ETHANOL	0.890	0.025	0.025	0.025	0.025	0.009	0.009	0.012

Stream	29	30	31	32
Temperature [°C]	30.0	30.0	92.5	50.0
Pressure [bar]	1.2	1.8	3.2	2.5
Mass Vapor Fraction	0	0.992	0	0
Mass Liquid Fraction	1	0.008	1	1
Mass Enthalpy [J/kg]	-1.5E+07	-9.0E+06	-6.3E+06	-6.4E+06
Mass Flow [kg/s]	12.20	0.31	2.19	2.19
Mass Fractions				
H2O	0.910	0.013	0.050	0.050
CO2	0.000	0.973	0.000	0.000
H3O+	1.4E-12	3.7E-09	4.8E-12	7.5E-12
K+	0.043	0.000	0.000	0.000
OH-	1.5E-05	1.0E-15	1.6E-16	2.7E-17
HCO3-	0.003	0.000	0.000	0.000
CO3--	0.032	0.000	0.000	0.000
ETHANOL	0.012	0.014	0.950	0.950

S3. Material and energy flows in ECCR system

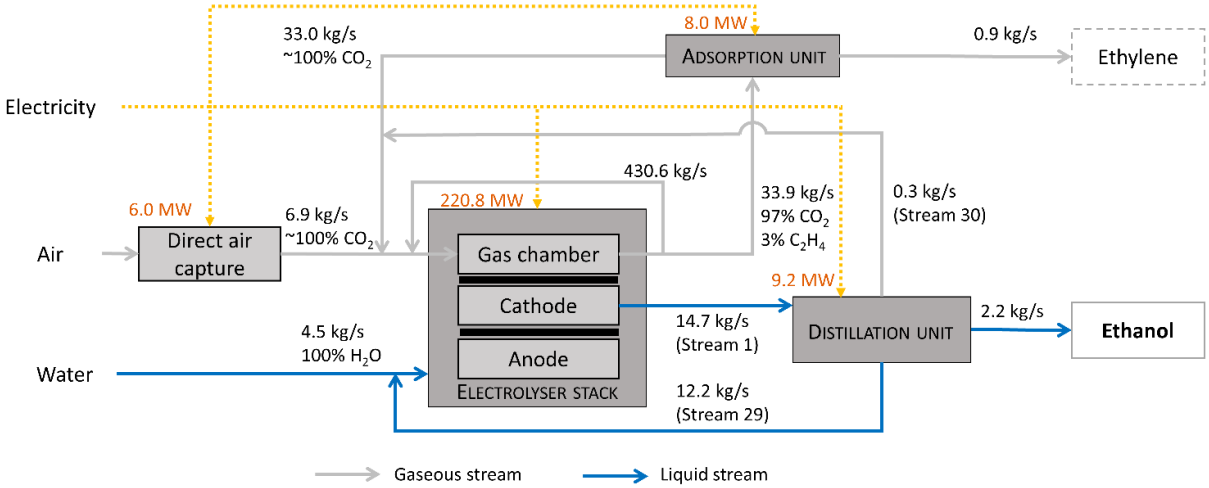

Figure S3. Material and energy flows in the entire electrocatalytic captured CO2 reduction (ECCR) system

Table S25. Carbon balance of system including recycled streams

Carbon in		**Carbon out**	
	kg/s		kg/s
CO_2 feed	125.16	Ethanol product	1.09
Electrolyte in	0.16	Ethylene product	0.78
		Distillation CO_2 recycle	0.08
		Adsorption CO_2 recycle	9.01
		Pre-adsorption recycle	114.20
		Electrolyte back	0.16
Total	125.32	**Total**	125.32

Removing recycle streams and specifying the inputs and outputs of the entire ECCR system including the DAC unit, the carbon balance is also met.

Table S26. Carbon balance of system with only inputs and outputs

Carbon in		**Carbon out**	
	kg/s		kg/s
Captured CO_2	1.87	Ethanol product	1.09
		Ethylene product	0.78
Total	1.87	**Total**	1.87

S4. Sensitivity analysis supplementary figures

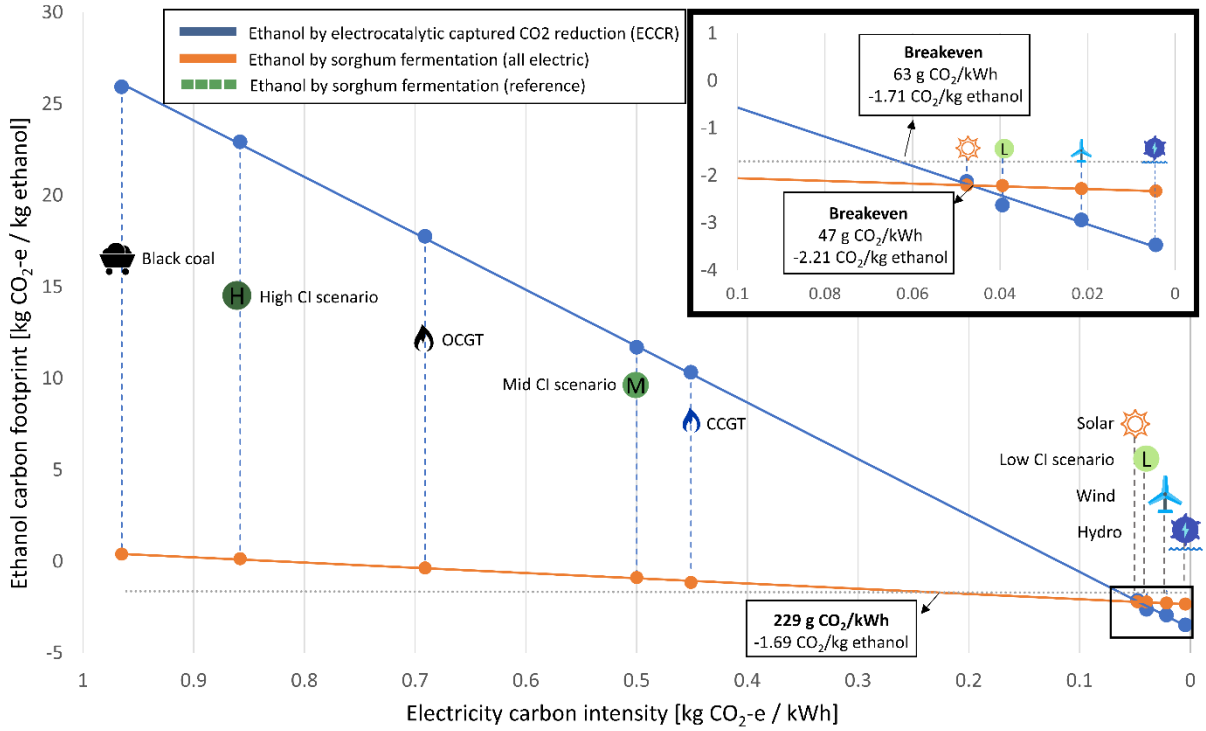

Figure S4. Carbon footprint of ethanol production by ECCR (blue line), by sorghum using only electricity (orange line), and by the reference sorghum process (dotted green line) with electricity of different sources and carbon intensity. Sorghum fermentation reference uses the average of using cottonseed and soybean meal as substitute for the dry distiller's grain with solubles (DDGS)

Icons for plot were taken from icons8.com and cleanpng.com

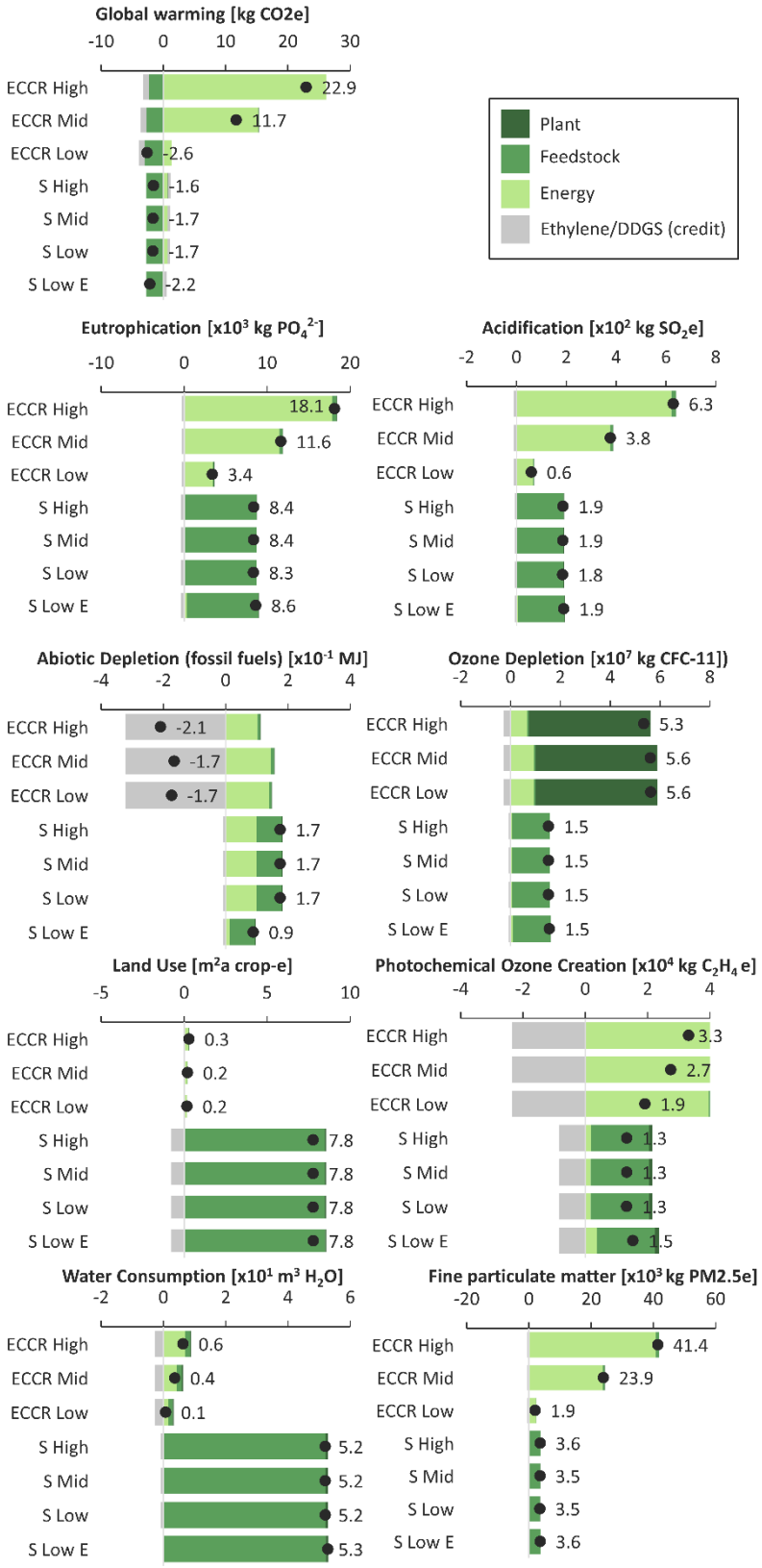

Figure S5. Potential environmental impacts in all categories for the electrocatalytic CO_2 reduction (ECCR) system and the sorghum bioethanol reference (with an average of cottonseed meal and soybean meal for the dry distiller's grains with solubles (DDGS) substitute) using electricity from the three carbon intensity (CI) scenarios and the fully electric bioethanol process using Low-CI electricity

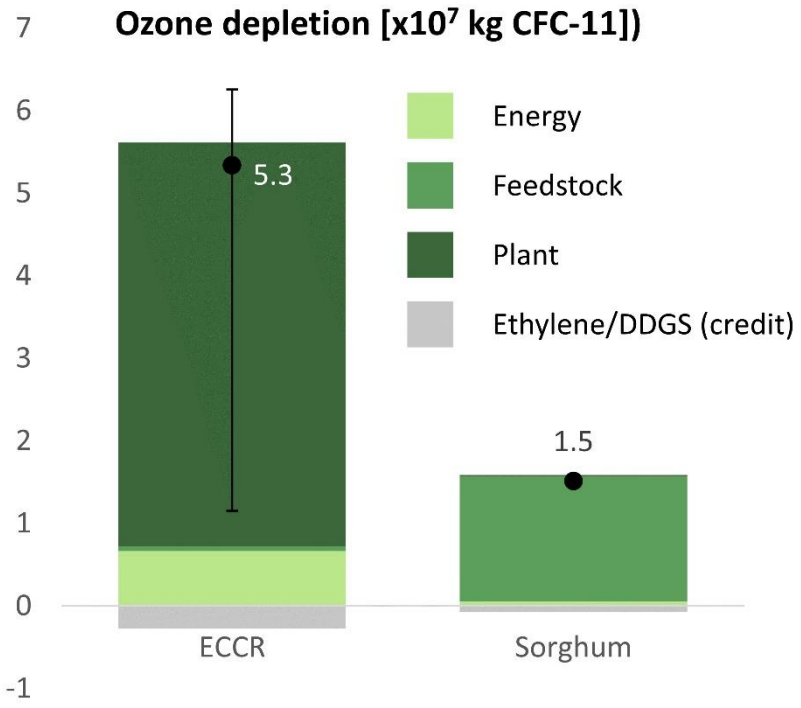

Figure S6. Sensitivity analysis on the effect of the PTFE membrane of the cathode to the ozone depletion potential compared to the reference. The range of PTFE membrane thickness is 30 – 270 μm

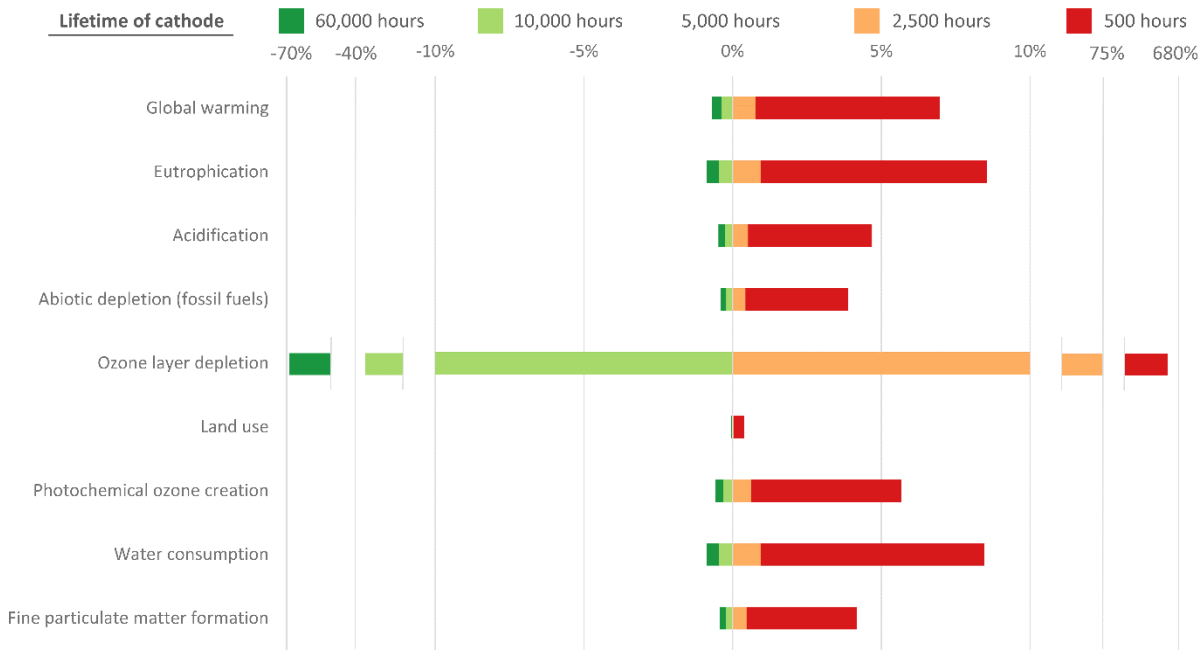

Figure S7. Sensitivity analysis on the effect of the lifetime of the catalyst in the ECCR system using the Low-CI scenario for all examined environmental impact categories. The range of the lifetime is 60,000 hours, 10,000 hours, 5,000 hours, 2,500 hours, and 500 hours.

The lifetime of the catalyst in this model was assumed to be 5,000 hours, as a conservative average stack lifetime of large-scale polymer electrolyte membrane fuel cells, which have a considerably shorter lifespan than alkaline systems (Myers et al., 2012). Figure S7 shows the effect on the environmental impacts by varying this parameter from 500 hours up to 60,000 hours, which is the lifetime of the rest of the components in the assembled electrolyser. The analysis indicates that, besides its effect on ODP, there is no significant difference in assuming a lifetime of 2,500 hours or 60,000 hours in the Low-Ci scenario. The difference in all impact categories between 2,500 and 60,000 hours is within only 2%. Even when the lifetime is reduced to 500 hours, there is an average increase of approximately 5% in all categories except ODP. The most sensitive category is the ODP, showing a decrease of 38% and 69% when increasing the lifetime to 10,000 and 60,000 hours, respectively. In contrast, the ODP increases in 75% and in 677% when the lifetime is reduced in half and in one order of magnitude, respectively.

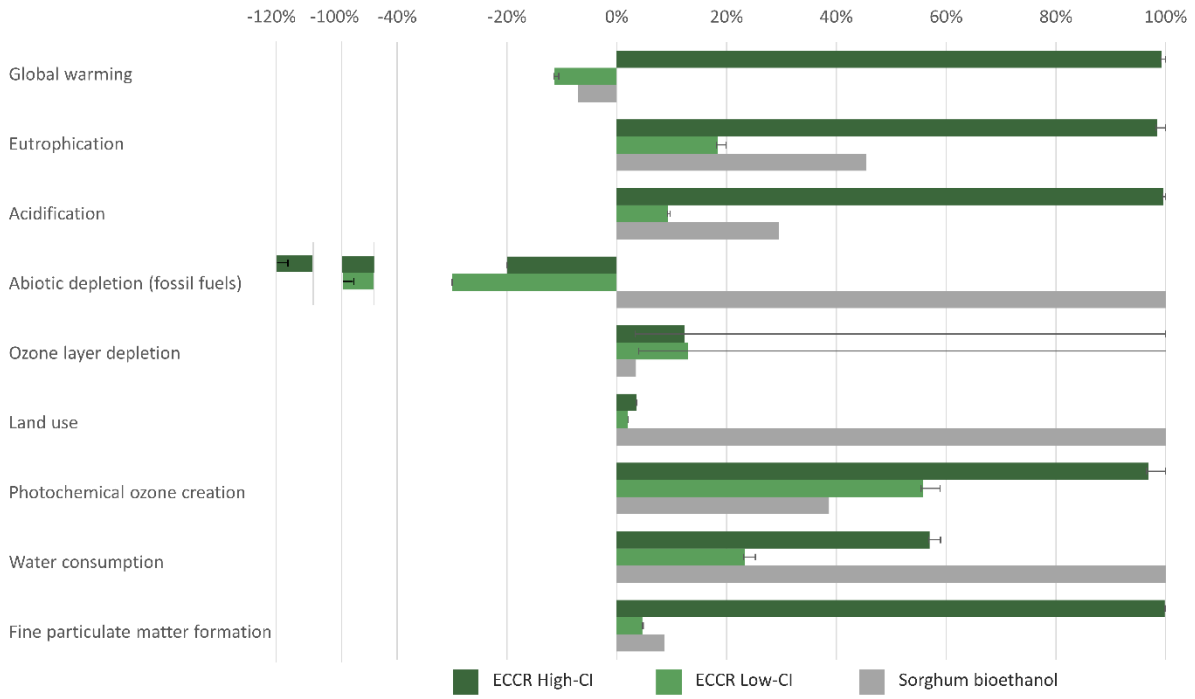

Figure S8. Sensitivity analysis on the effect of the lifetime of the catalyst in the ECCR system cathode using High and Low carbon intensity (High-CI and Low-CI) electricity scenarios for all examined environmental impact categories. Bars show impact at a lifetime of 5,000 hours with error bars for a lifetime of 500 hours to 60,000 hours. With the exception of ozone layer depletion (ODP), the difference between the impact of 5,000- and 60,000-hours catalyst lifetime is marginal

References

Australian Life Cycle Assessment Society, 2020. Australian Life Cycle Initiative Database V1.35.

Beccali, M., Cellura, M., Longo, S., Finocchiaro, P., Selke, T., 2014. IEA Report on LCA. Vienna.

Bertuccioli, L., Chan, A., Hart, D., Lehner, F., Madden, B., Standen, E., 2014. Development of water electrolysis in the European Union, Fuel Cells and Hydrogen Joint Undertaking. Cambridge.

Blom, M.J.W., van Swaaij, W.P.M., Mul, G., Kersten, S.R.A., 2019. Overall mass balance evaluation of electrochemical reactors: The case of CO2 reduction. Electrochim. Acta 333, 135460. https://doi.org/10.1016/j.electacta.2019.135460

Carmo, M., Fritz, D.L., Mergel, J., Stolten, D., 2013. A comprehensive review on PEM water electrolysis. Int. J. Hydrogen Energy 38, 4901–4934. https://doi.org/10.1016/j.ijhydene.2013.01.151

Casas, N., Schell, J., Pini, R., Mazzotti, M., 2012. Fixed bed adsorption of CO 2/H 2 mixtures on activated carbon: Experiments and modeling. Adsorption 18, 143–161. https://doi.org/10.1007/s10450-012-9389-z

Chaudhari, N.K., Jin, H., Kim, B., Lee, K., 2017. Nanostructured materials on 3D nickel foam as electrocatalysts for water splitting. Nanoscale 9, 12231–12247. https://doi.org/10.1039/c7nr04187j

Chen, C.C., Song, Y., 2004. Generalized electrolyte-NRTL model for mixed-solvent electrolyte systems. AIChE J. 50, 1928–1941. https://doi.org/10.1002/aic.10151

Dinh, C.T., Burdyny, T., Kibria, G., Seifitokaldani, A., Gabardo, C.M., Pelayo García De Arquer, F., Kiani, A., Edwards, J.P., De Luna, P., Bushuyev, O.S., Zou, C., Quintero-Bermudez, R., Pang, Y., Sinton, D., Sargent, E.H., 2018. CO2 electroreduction to ethylene via hydroxide-mediated copper catalysis at an abrupt interface. Science (80-.). 360, 783–787. https://doi.org/10.1126/science.aas9100

Duclos, L., Lupsea, M., Mandil, G., Svecova, L., Thivel, P.X., Laforest, V., 2017. Environmental assessment of proton exchange membrane fuel cell platinum catalyst recycling. J. Clean. Prod. 142, 2618–2628. https://doi.org/10.1016/j.jclepro.2016.10.197

Edge Environment, Lifecycles, 2016. Method and guidance for undertaking life cycle assessment (LCA) of bioenergy products and projects. Rep. Aust. Renew. Energy Agency.

Evangelisti, S., Tagliaferri, C., Brett, D.J.L., Lettieri, P., 2017. Life cycle assessment of a polymer electrolyte membrane fuel cell system for passenger vehicles. J. Clean. Prod. 142, 4339–4355. https://doi.org/10.1016/j.jclepro.2016.11.159

Farrell, R., Santella, R., 2019. Australia: Biofuels Annual 2018. Canberra.

Google, n.d. Manual measured area around Dalby Biorefinery [WWW Document]. URL https://www.google.com.au/maps/place/Dalby+Bio-Refinery/@-27.1467345,151.2392505,1237m/data=!3m1!1e3!4m5!3m4!1s0x6bbdf9ed5453f711:0x70725f84da5e0754!8m2!3d-27.1455431!4d151.2454315 (accessed 11.12.20).

Grant, T., Cruypenninck, H., Eady, S., Mata, G., 2014. AusAgLCI methodology for developing Life Cycle Inventory. Canberra.

Harkin, T., 2012. Multi-Objective Optimisation of CCS using simulation, heat integration and cost estimation. doctoral thesis, Monash University.

Harned, H.S., Davis, R., 1943. The Ionization Constant of Carbonic Acid in Water and the Solubility of Carbon Dioxide in Water and Aqueous Salt Solutions from 0 to 50°. J. Am. Chem. Soc. 65, 2030–2037. https://doi.org/10.1021/ja01250a059

Harned, H.S., Scholes, S.R., 1941. The Ionization Constant of HCO3- from 0 to 50°. J. Am. Chem. Soc. 63, 1706–1709. https://doi.org/10.1021/ja01851a058

Holmes, G., Keith, D.W., 2012. An air-liquid contactor for large-scale capture of CO2 from air. Philos. Trans. R. Soc. A Math. Phys. Eng. Sci. 370, 4380–4403. https://doi.org/10.1098/rsta.2012.0137

Hori, Y., 2008. Electrochemical CO2 Reduction on Metal Electrodes, in: Vayenas, C.G., White, R.E., Gamboa-Aldeco, M.E. (Eds.), Modern Aspects of Electrochemistry. Springer New York, New York, pp. 89–189. https://doi.org/10.1007/978-0-387-49489-0_3

Hudkins, J.R., Wheeler, D.G., Peña, B., Berlinguette, C.P., 2016. Rapid prototyping of electrolyzer flow field plates. Energy Environ. Sci. 9, 3417–3423. https://doi.org/10.1039/c6ee01997h

Hung, C.-J., Liu, C.-H., Wang, C.-H., Chen, W.-H., Shen, C.-W., Liang, H.-C., Ko, T.-H., 2015. Effect of conductive carbon material content and structure in carbon fiber paper made from carbon felt on the performance of a proton exchange membrane fuel cell. Renew. Energy 78, 364–373. https://doi.org/https://doi.org/10.1016/j.renene.2015.01.021

Keith, D.W., Holmes, G., St. Angelo, D., Heidel, K., 2018. A Process for Capturing CO2 from the Atmosphere. Joule 2, 1573–1594. https://doi.org/10.1016/j.joule.2018.05.006

Klinger Australia, n.d. Klinger SOFT-CHEM [WWW Document]. URL https://www.klinger.com.au/products/ptfe-gasket-materials/klinger-soft-chem (accessed 11.22.20).

Koj, J.C., Schreiber, A., Zapp, P., Marcuello, P., 2015. Life Cycle Assessment of Improved High Pressure Alkaline Electrolysis, STE Research Report. https://doi.org/10.1016/j.egypro.2015.07.576

Li, F., Li, Y.C., Wang, Z., Li, J., Nam, D.H., Lum, Y., Luo, M., Wang, X., Ozden, A., Hung, S.F., Chen, B., Wang, Yuhang, Wicks, J., Xu, Y., Li, Y., Gabardo, C.M., Dinh, C.T., Wang, Ying, Zhuang, T.T., Sinton, D., Sargent, E.H., 2020. Cooperative CO2-to-ethanol conversion via enriched intermediates at molecule–metal catalyst interfaces. Nat. Catal. 3, 75–82. https://doi.org/10.1038/s41929-019-0383-7

Li, H., Oloman, C., 2005. The electro-reduction of carbon dioxide in a continuous reactor. J. Appl. Electrochem. 35, 955–965. https://doi.org/10.1007/s10800-005-7173-4

Liang, Y., Liu, Q., Asiri, A.M., Sun, X., He, Y., 2015. Nickel-iron foam as a three-dimensional robust oxygen evolution electrode with high activity. Int. J. Hydrogen Energy 40, 13258–13263. https://doi.org/10.1016/j.ijhydene.2015.07.165

Liu, C.M., Sandhu, N.K., McCoy, S.T., Bergerson, J.A., 2020. A life cycle assessment of greenhouse gas emissions from direct air capture and Fischer-Tropsch fuel production. Sustain. Energy Fuels 4, 3129–3142. https://doi.org/10.1039/c9se00479c

Liu, P.S., Liang, K.M., 2000. Preparation and corresponding structure of nickel foam. Mater. Sci. Technol. 16, 575–578. https://doi.org/10.1179/026708300101508108

Liu, W., Du, K., Liu, L., Zhang, J., Zhu, Z., Shao, Y., Li, M., 2017. One-step electroreductively deposited iron-cobalt composite films as efficient bifunctional electrocatalysts for overall water splitting. Nano Energy 38, 576–584. https://doi.org/10.1016/j.nanoen.2016.11.047

Ma, M., Clark, E.L., Therkildsen, K.T., Dalsgaard, S., Chorkendorff, I., Seger, B., 2020. Insights into the carbon balance for CO2 electroreduction on Cu using gas diffusion electrode reactor designs. Energy Environ. Sci. 13, 977–985. https://doi.org/10.1039/d0ee00047g

Majeau-Bettez, G., Hawkins, T.R., Strømman, A.H., 2011. Life Cycle Environmental Assessment of Lithium-Ion and Nickel Metal Hydride Batteries for Plug-In Hybrid and Battery Electric Vehicles. Environ. Sci. Technol. 45, 4548–4554. https://doi.org/10.1021/es103607c

Maring, B.J., Webley, P.A., 2013. A new simplified pressure/vacuum swing adsorption model for rapid adsorbent screening for CO2 capture applications. Int. J. Greenh. Gas Control 15, 16–31. https://doi.org/10.1016/j.ijggc.2013.01.009

Microlab Scientific, n.d. Hydrophobic PTFE Membrane Filter [WWW Document]. URL http://www.microlabscientific.com/Hydrophobic-PTFE-Membrane-Filter.html (accessed 4.12.21).

Millero, F.J., 1995. Thermodynamics of the carbon dioxide system in the oceans. Geochim. Cosmochim. Acta 59, 661–677. https://doi.org/https://doi.org/10.1016/0016-7037(94)00354-O

Myers, A.L., Prausnitz, J.M., 1965. Thermodynamics of mixed-gas adsorption. AIChE J. 11, 121–127. https://doi.org/10.1002/aic.690110125

Myers, D.J., Wang, X., Kariuki, N., DeCrane, S., Nowicki, T., Arisetty, S., Subbaraman, R., Ahluwalia, R., Gilbert, J.A., Puchala, B., Holby, E., Morgan, D., Ball, S.C., Sharman, J., Theobald, B., Hards, G.A., Gummalla, M., Z. Yang, S., Han, B., 2012. Polymer Electrolyte Fuel Cell Lifetime Limitations: The Role of Electrocatalyst Degradation, ECS Meeting Abstracts. https://doi.org/10.1149/MA2012-02/13/1276

Pan, Z.F., An, L., Zhao, T.S., Tang, Z.K., 2018. Advances and challenges in alkaline anion exchange membrane fuel cells. Prog. Energy Combust. Sci. 66, 141–175. https://doi.org/10.1016/j.pecs.2018.01.001

Park, S., Lee, J.-W., Popov, B.N., 2008. Effect of PTFE content in microporous layer on water management in PEM fuel cells. J. Power Sources 177, 457–463. https://doi.org/https://doi.org/10.1016/j.jpowsour.2007.11.055
Queensland Government, 2017. Dalby Biorefinery Ltd, Advanced Manufacturing | Sustainable Manufacturing in Action.
Reich, R., Ziegler, W.T., Rogers, K.A., 1980. Adsorption of Methane, Ethane, and Ethylene Gases and Their Binary and Ternary Mixtures and Carbon Dioxide on Activated Carbon at 212-301 K and Pressures to 35 Atmospheres. Ind. Eng. Chem. Process Des. Dev. 19, 336–344. https://doi.org/10.1021/i260075a002
Rumayor, M., Dominguez-Ramos, A., Irabien, A., 2019. Environmental and economic assessment of the formic acid electrochemical manufacture using carbon dioxide: Influence of the electrode lifetime. Sustain. Prod. Consum. 18, 72–82. https://doi.org/10.1016/j.spc.2018.12.002
Schmidt, O., Gambhir, A., Staffell, I., Hawkes, A., Nelson, J., Few, S., 2017. Future cost and performance of water electrolysis: An expert elicitation study. Int. J. Hydrogen Energy 42, 30470–30492. https://doi.org/10.1016/j.ijhydene.2017.10.045
Sharp, K., 2020. Personal communication.
Simons, A., Bauer, C., 2015. A life-cycle perspective on automotive fuel cells. Appl. Energy 157, 884–896. https://doi.org/10.1016/j.apenergy.2015.02.049
Stumm, W., Morgan, J.J., 1995. Aquatic Chemistry: Chemical Equilibria and Rates in Natural Waters, 3rd editio. ed. https://doi.org/10.1094/asbcmoa-beer-13
Tan, Y.C., Lee, K.B., Song, H., Oh, J., 2020. Modulating Local CO2 Concentration as a General Strategy for Enhancing C−C Coupling in CO2 Electroreduction. Joule 4, 1104–1120. https://doi.org/10.1016/j.joule.2020.03.013
United Petroleum, n.d. Dalby Gas Pipeline [WWW Document]. URL https://www.unitedpetroleum.com.au/dalby-bio-refinery/dalby-gas-pipeline/ (accessed 10.24.20).
Viebahn, P., Scholz, A., Zelt, O., 2019. German Energy Research Program — Results of a Multi-Dimensional Analysis. Energies 18, 1–27.
Wang, X., Wang, Z., García de Arquer, F.P., Dinh, C.T., Ozden, A., Li, Y.C., Nam, D.H., Li, J., Liu, Y.S., Wicks, J., Chen, Z., Chi, M., Chen, B., Wang, Y., Tam, J., Howe, J.Y., Proppe, A., Todorović, P., Li, F., Zhuang, T.T., Gabardo, C.M., Kirmani, A.R., McCallum, C., Hung, S.F., Lum, Y., Luo, M., Min, Y., Xu, A., O'Brien, C.P., Stephen, B., Sun, B., Ip, A.H., Richter, L.J., Kelley, S.O., Sinton, D., Sargent, E.H., 2020. Efficient electrically powered CO2-to-ethanol via suppression of deoxygenation. Nat. Energy 5, 478–486. https://doi.org/10.1038/s41560-020-0607-8
Weisenberger, S., Schumpe, A., 1996. Estimation of Gas Solubilities in Salt Solutions at Temperatures from 273 K to 363 K. AIChE J. 42, 298–300. https://doi.org/10.1002/aic.690420130
Wernet, G., Bauer, C., Steubing, B., Reinhard, J., Moreno-Ruiz, E., Weidema, B., 2016. The ecoinvent database version 3 (part I): overview and methodology. Int. J. Life Cycle Assess. 21, 1218–1230. https://doi.org/10.1007/s11367-016-1087-8
Wernet, G., Lévová, T., Bourgault, G., Valsasina, L., Fitzgerald, D., Moreno Ruiz, E., 2017. Data on Production of Chemicals created for the EU Product Environmental Footprint (PEF) pilot phase implementation. Zürich, Switzerland.
Wisz, M.W., Antonelli, R., Ragi, E.G., 1981. High Performance Trays and Heat Exchangers in Heat Pumped Distillation Columns, in: Third Industrial Energy Technology Conference. Houston, TX, pp. 91–96.
Yacout, D.M.M., Abd El-Kawi, M.A., Hassouna, M.S., 2016. Cradle to gate environmental impact assessment of acrylic fiber manufacturing. Int. J. Life Cycle Assess. 21, 326–336. https://doi.org/10.1007/s11367-015-1023-3
Zandvoort, I. van, Ras, E.J., de Graaf, R., Krishna, R., 2020. Using transient breakthrough experiments for screening of adsorbents for separation of C2H4/CO2 mixtures. Sep. Purif. Technol. 241, 116706. https://doi.org/10.1016/j.seppur.2020.116706
Zhang, F., Zhang, H., Qu, C., 2011. Imidazolium functionalized polysulfone anion exchange membrane for fuel cell application. J. Mater. Chem. 21, 12744–12752. https://doi.org/10.1039/c1jm10656b
Zhong, H., Fujii, K., Nakano, Y., Jin, F., 2015. Effect of CO2 bubbling into aqueous solutions used for

electrochemical reduction of CO2 for energy conversion and storage. J. Phys. Chem. C 119, 55–61. https://doi.org/10.1021/jp509043h